WT-1602(EX)
EXTRACTED VERSION

OPERATION HARDTACK—PROJECT 2.14

Fallout Contamination from a Very Low Yield Burst

410999

M. Cowan, Jr.
Sandia Corporation
Albuquerque, NM

8 May 1962

NOTICE:
This is an extract of WT-1602, Operation HARDTACK, Project 2.14.

Extracted version prepared for
Director
DEFENSE NUCLEAR AGENCY
Washington, DC 20305-1000

1 September 1985

REPORT DOCUMENTATION PAGE

1a REPORT SECURITY CLASSIFICATION UNCLASSIFIED	1b RESTRICTIVE MARKINGS
2a SECURITY CLASSIFICATION AUTHORITY N/A since Unclassified	3 DISTRIBUTION/AVAILABILITY OF REPORT Approved for public release; distribution is unlimited.
2b DECLASSIFICATION/DOWNGRADING SCHEDULE N/A since Unclassified	
4 PERFORMING ORGANIZATION REPORT NUMBER(S)	5 MONITORING ORGANIZATION REPORT NUMBER(S) WT-1602(EX)
6a NAME OF PERFORMING ORGANIZATION Sandia Corporation 6b OFFICE SYMBOL (If applicable)	7a NAME OF MONITORING ORGANIZATION Defense Atomic Support Agency
6c ADDRESS (City, State, and ZIP Code) Albuquerque, NM	7b ADDRESS (City, State, and ZIP Code) Washington, DC
8a NAME OF FUNDING/SPONSORING ORGANIZATION 8b OFFICE SYMBOL (If applicable)	9 PROCUREMENT INSTRUMENT IDENTIFICATION NUMBER
8c ADDRESS (City, State, and ZIP Code)	10 SOURCE OF FUNDING NUMBERS PROGRAM ELEMENT NO / PROJECT NO / TASK NO / WORK UNIT ACCESSION NO

11 TITLE (Include Security Classification)
OPERATION HARDTACK—PROJECT 2.14
Fallout Contamination from a Very Low Yield Burst, Extracted Version

12 PERSONAL AUTHOR(S)
Cowan, M., Jr.

13a TYPE OF REPORT	13b TIME COVERED FROM ____ TO ____	14 DATE OF REPORT (Year, Month, Day)	15 PAGE COUNT
		620508	64

16 SUPPLEMENTARY NOTATION This report has had sensitive military information removed in order to provide an unclassified version for unlimited distribution. The work was performed by the Defense Nuclear Agency in support of the DoD Nuclear Test Personnel Review Program.

17 COSATI CODES			18 SUBJECT TERMS (Continue on reverse if necessary and identify by block number)
FIELD	GROUP	SUB-GROUP	Hardtack Low Yield Bursts Fallout Contamination
18	3		
18	8		

19 ABSTRACT (Continue on reverse if necessary and identify by block number)

The primary objective of this project was to determine the military significance of fallout contamination from small-yield fission weapons.

The specific objectives were to (1) make the necessary measurements during Shot Fig to delineate the fallout gamma-radiation field produced by a land-surface detonation of a fission weapon; (2) use data collected to construct a fallout model for use with any wind pattern, and evaluate extremes in militarily significant contamination intensities for the same yield range; and (3) define the attendant plutonium contamination problem.

A dynamic close-in fallout model is presented for yields of 1 to 100 tons, which accounts for growth and drift of the cloud during its rise and is consistent with Fig measurements of cloud shine and amount of activity deposited, together with dose-rate intensity as functions of downwind distance.

20 DISTRIBUTION/AVAILABILITY OF ABSTRACT	21 ABSTRACT SECURITY CLASSIFICATION
☒ UNCLASSIFIED/UNLIMITED ☐ SAME AS RPT ☐ DTIC USERS	UNCLASSIFIED
22a NAME OF RESPONSIBLE INDIVIDUAL Mark D. Flohr	22b TELEPHONE (Include Area Code) (202) 325-7559 / 22c OFFICE SYMBOL DNA/ISCM

FOREWORD

Classified material has been removed in order to make the information available on an unclassified, open publication basis, to any interested parties. The effort to declassify this report has been accomplished specifically to support the Department of Defense Nuclear Test Personnel Review (NTPR) Program. The objective is to facilitate studies of the low levels of radiation received by some individuals during the atmospheric nuclear test program by making as much information as possible available to all interested parties.

The material which has been deleted is either currently classified as Restricted Data or Formerly Restricted Data under the provisions of the Atomic Energy Act of 1954 (as amended), or is National Security Information, or has been determined to be critical military information which could reveal system or equipment vulnerabilities and is, therefore, not appropriate for open publication.

The Defense Nuclear Agency (DNA) believes that though all classified material has been deleted, the report accurately portrays the contents of the original. DNA also believes that the deleted material is of little or no significance to studies into the amounts, or types, of radiation received by any individuals during the atmospheric nuclear test program.

OPERATION HARDTACK — PROJECT 2.14

FALLOUT CONTAMINATION FROM A VERY-LOW-YIELD BURST

M. Cowan, Jr.

Sandia Corporation
Albuquerque, New Mexico

ABSTRACT

Fallout measurements were made during Shot Fig to determine military significance of fallout contamination from small-yield fission weapons. Results indicate that, when the scaling techniques in TM 23-200 (1957 edition) are extended to gross overestimates of downwind extent are made for H + 1 hour intensities of 100 r/hr or less.

A dynamic close-in fallout model is presented for yields of 1 to 100 tons, which accounts for growth and drift of the cloud during its rise and is consistent with Fig measurements of cloud shine and amount of activity deposited together with dose-rate intensity as functions of downwind distance.

Calculations using this model are made for windspeeds of 5, 15, and 30 knots. Intensities greater than 100 r/hr show an increase, whereas intensities less than 100 r/hr show a decrease in downwind extent with decreasing windspeed. However the 100-r/hr intensity will extend no farther downwind than 600 to 700 feet

The few measurements of plutonium contamination indicate that no serious long-term problem will result from this source after the nuclear detonation of a small-yield fission device.

FOREWORD

This report presents the final results of one of the projects participating in the military-effect programs of Operation Hardtack. Overall information about this and the other military-effect projects can be obtained from ITR-1660, the "Technical Summary of Military Effects, Programs 1-9 (DASA)." This technical summary includes: (1) tables listing each detonation with its yield, type, environment, meteorological conditions, etc.; (2) maps showing shot locations; (3) discussions of results by programs; (4) summaries of objectives, procedures, results, etc., for all projects; and (5) a listing of project reports for the military-effect programs.

CONTENTS

TABLES

FIGURES

Chapter 1

INTRODUCTION

1.1 OBJECTIVES

The primary objective was to determine the military significance of fallout contamination from small-yield fission weapons.

The specific objectives were to (1) make the necessary measurements during Shot Fig to delineate the fallout gamma-radiation field produced by a land-surface detonation of a fission weapon (2) use data collected to construct a fallout model for use with any wind pattern, and evaluate extremes in militarily significant contamination intensities for the same yield range; and (3) define the attendant plutonium contamination problem.

1.2 BACKGROUND

1.2.1 Reason for Fallout Measurements. Small-yield fission weapons (10 to 100 tons) are being considered for use by the lowest echelons of the Army and Marines. For this application a minimum of residual contamination, especially windborne fallout, is essential. If a serious fallout radiation problem results from a surface burst of such small-yield weapons, it may be necessary to fuze for an airburst, thereby sacrificing obvious advantages of manufacturing, maintenance, and field use offered by contact fuzing. Estimates of fallout contamination made by extrapolating existing data are questionable.

1.2.2 Estimates from Other Yields. The fallout radiation field that could result from a surface burst in the 10- to 100-ton range may be estimated from experience gained from other yields and from the following assumptions: (1) cloud dimensions for the yield of interest can be estimated with reasonable accuracy; (2) vertical space distribution of activity within the cloud is similar for the yield range involved, that is, the same percentage of total activity is located within the same relative vertical cloud increment; and (3) at the same relative cloud height, fall-rate distribution of activity is the same for all clouds.

1.2.3 Fallout Model Used for Test Operations. The vast majority of fallout data has come from tests on towers at Nevada Test Site (NTS) for the yield range of 10 to 50 kt. From this experience a fallout model has evolved, which consists of vertical space-and-fall-rate distribution for the activity in the stabilized cloud. By use of this model and wind velocity predictions for altitudes of interest, expected fallout patterns are calculated prior to each shot of a test operation as a standard safety practice. Comparison of measured fallout patterns with those calculated, using best available measurements of actual post-shot wind conditions, indicates that intensity and shape of surface contamination are well

described at distances ranging from 25 to 250 miles from ground zero. An evaluation of the model for points closer to ground zero has been hampered by lack of data. Also, the assumption of a stabilized, fully developed cloud over ground zero at zero time is usually made for calculations utilizing this model, since this assumption is good for calculating intensities at points of primary concern around NTS. However, for small yields and fallout intensities high enough to be of military importance, all particle trajectories, including rise and fall, must be considered. Figures 1.1 and 1.2 show space-and-fall-rate distributions of the model used for fallout prediction during Operation Hardtack. The advantage of a model of this kind is that it may be used to estimate the influence of different wind conditions on surface contamination intensities.

1.2.4 Model Calculations for a Surface Burst. On the basis of the assumptions stated above, the fallout pattern of a surface burst was calculated, using the Hardtack model, for the wind condition expected for Shot Fig. Results are shown in Figure 1.3. A hodograph for the expected wind structure is shown in Figure 1.4. (Hodographs are described in Section 1.3.2.)

Since calculated intensities are sensitive to the cloud geometry chosen, it is important to make a realistic estimate of cloud dimensions. Cloud dimensions used are summarized in Table 1.1. The cloud was assumed to be fully developed and stabilized over ground zero at zero time.

It should be understood that slight variations in burst environment can cause large variations in cloud dimensions, with attendant changes in the fallout intensities. For example, uncertainty in cloud height is indicated in Figure 1.5 by the broad band necessary to cover data points of cloud height versus yield. Variations in burst environment apparently can affect cloud heights to the extent of a tenfold change in yield. The shaded region shown in Figure 1.5 indicates the range of cloud heights possible from a nuclear detonation within a yield range of 10 to 100 tons.

1.2.5 Estimates from Geometric Scaling. Fallout contamination for discrete wind situations can also be estimated by a relatively simple geometric scaling method (References 1 and 2). In this method a measured contamination pattern from one yield is scaled to that expected for another in a manner consistent with the assumptions stated above. The usual practice in this method is to assume that linear dimensions of clouds scale as the cube root of yield. Then, linear dimensions of a given surface contamination contour as well as the intensity label on that contour are scaled as the cube root of yield.

The advantage of this method is that details of space and fall-rate distributions of activity within the cloud are unnecessary.

Best results are expected when the yield range covered is minimized. The two land surface shots from which fallout information has been obtained nearest the yield range of 10 to 100 tons were Coulomb C of Operation Plumbbob at 600 tons and another one-point detonation 18 January 1956, Results of scaling data from both shots by this simple geometric method are compared in Figure 1.6. Also shown for comparison are intensity-distance curves taken from the Hardtack model calculation (Figure 1.3) and from an extrapolation of prediction curves given in Reference 1. Wind velocity differences may have been sufficient to account for some of the difference between estimates based on these two events; also, the assumptions made as the basis of the scaling method may not be valid over the yield range of to 600 tons. Higher estimated intensities are obtained when scaling from the higher yield. Experience with nonnuclear one-point detonations suggests that this may be due to a lower mean fall rate (smaller size) for the contamination

from the smaller yield (Reference 3). The curves from Reference 1 and from the Hardtack model calculations are both based on experience gained from yields greater than 1 kt.

1.3 THEORY

1.3.1 Influence of Wind on Fallout Contamination. When a nuclear detonation occurs on the ground, fission products become associated with particles of soil, which differ in size, fall rate, and amount of activity collected. These particles are drawn up by the rising hot gases that result from the detonation and are distributed throughout the cloud that is formed.

When equilibrium between the cloud and the surrounding atmosphere has been established, particles are free to settle to the surface. During the settling period, horizontal motions will be governed by the wind velocities experienced. Thus, the wind structure from the surface to the top of the cloud determines to a large extent the location and intensity of resulting surface contamination.

Since a single test can be made for only one wind condition, it is important to know what will happen for other wind conditions, particularly those leading to extremes in militarily significant contamination levels. If answers to these questions are to be established, a model consisting of space-and-fall-rate distributions for the activity in the cloud must be obtained.

1.3.2 Hodographs. Figure 1.7 shows an example of a convenient method of schematically picturing the effect of a particular wind condition on fallout particles. The curved line, ABCDEF, called a hodograph, represents the projected path of a balloon as it rises through the wind structure at a constant rate of ascent. Since the balloon is continually rising, each point of the hodograph is representative of its plan position at a specific altitude. Radiating vectors are drawn through Altitudes A, B, C, D, E, and F. Point C, for example, is the plan position of the balloon when it has reached Altitude C. The mean horizontal windspeed from Altitude C to the surface is given by the distance OC divided by the elapsed time taken by the balloon to reach Altitude C. Particles that descend from a position over zero at Altitude C will land at Point C on the hodograph, provided the rate of descent is constant and equal to the rise rate of the balloon.

Therefore, a hodograph is also the locus of final positions on the ground of particles that descend through a given wind structure at a particular constant rate from points at different altitudes directly over ground zero. Different constant rates of descent describe similarly shaped hodographs of greater or lesser extent so that a straight line drawn from ground zero through a specific altitude on one hodograph intersects all others at the same altitude. Such a line is called a height line.

Under certain conditions, measured surface contamination levels may be used with the measured hodograph to construct the space-and-fall-rate distribution necessary for a fallout model (Reference 3).

1.3.3 Surface Measurements and Fall Rate of the Activity. In general, the intensity of fallout radiation I for a point on the surface is given by

$$I = \int\int A(h, f)\, dh\, df \qquad (1.1)$$

Where: A = activity density per unit fall-rate interval in the cloud, curies-hr/ft^4
h = cloud height, feet
f = fall rate of the activity, ft/hr

A(h, f) and I are measured at the same time. When A(h, f) is known, I may be calculated for any point once the contributing altitudes and fall rates are obtained from a particular hodograph and the cloud dimensions.

Also, estimates of the amount of fallout activity collected by an air sampler operating at a given location in the fallout field may be made from the fallout model for any particular wind situation. Let C(t) be the activity density in the air at a location in the fallout field, and B be the air sampling rate. The amount of fallout activity collected from air sampled during the time of fallout is then u. Therefore,

$$u = B \int_{t=0}^{t=T} C(t)dt \tag{1.2}$$

Where: t = time measured from the start of fallout to its cessation at t = T

During fallout arrival, activity density in air near the surface is caused by a slice of cloud dh thick, which has fallen from h and which contains particulate matter covering a small range of fall rates from f to f + df.

The time for this thin slice to fall dh past a point near the surface is

$$dt = \frac{dh}{f} \tag{1.3}$$

During this time, the activity density will be the same as that which existed in the cloud at altitude h on fall rates from f to f + df, provided cloud dimensions do not change appreciably with time. Therefore,

$$u = B \iint A \frac{(h, f)dfdh}{f} \tag{1.4}$$

comparison of Equations 1.1 and 1.4 reveals an important relationship between I and u, which depends on the fall rate of the contaminating particle. If the range of fall rates that may contribute to a given point is small compared to $\bar{f}$, the mean fall rate contributing, then

$$\bar{f} = B \frac{I}{u} \tag{1.5}$$

TABLE 1.1 POSSIBLE CLOUD DIMENSIONS

Cloud height	5,500 feet
Puff diameter	2,000 feet
Stem diameter	1,000 feet
Ratio of stem to puff height	4

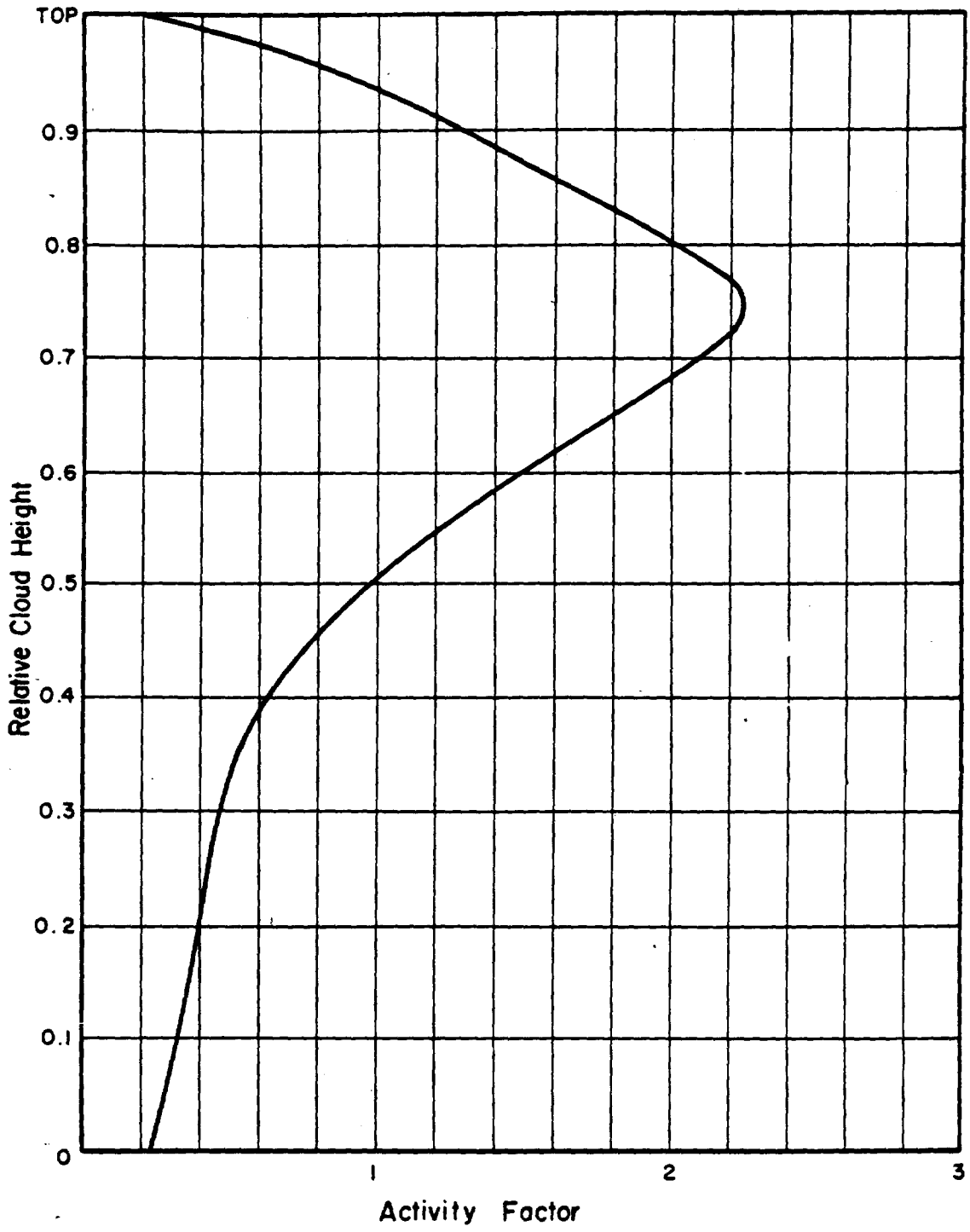

Figure 1.1 Hardtack model space distribution. For a uniform distribution of activity with height activity, the factor would equal 1 for all heights.

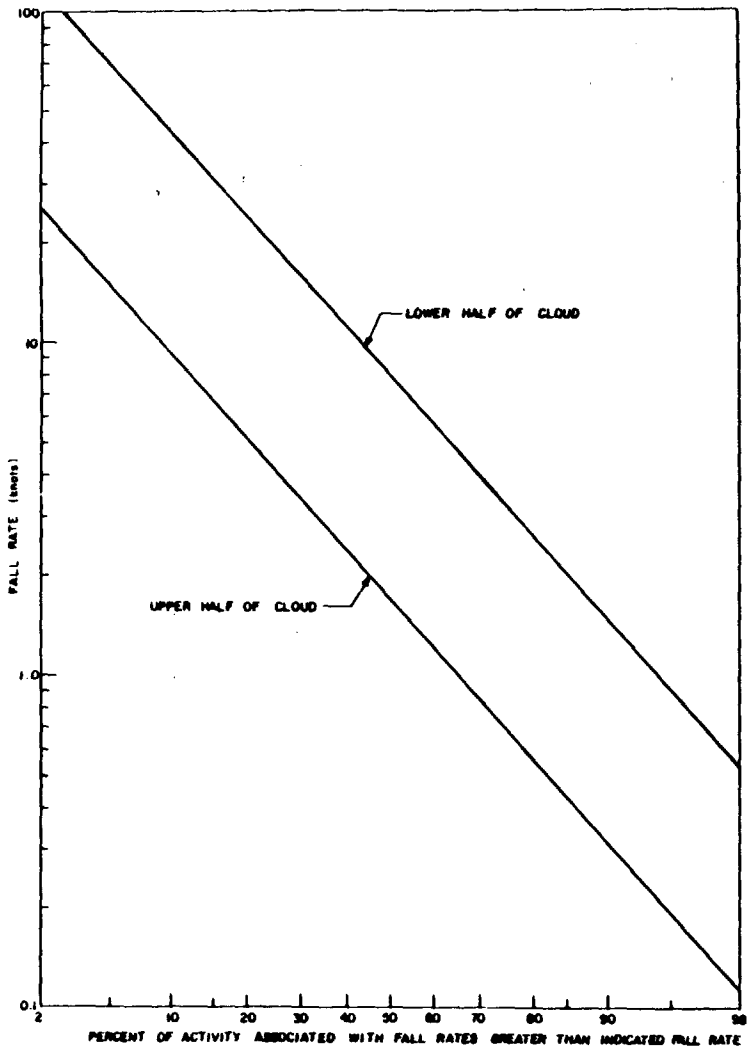

Figure 1.2 Hardtack model fall-rate distribution. Distributions are log-normal with $\sigma = 1.3$ and indicated median fall rates.

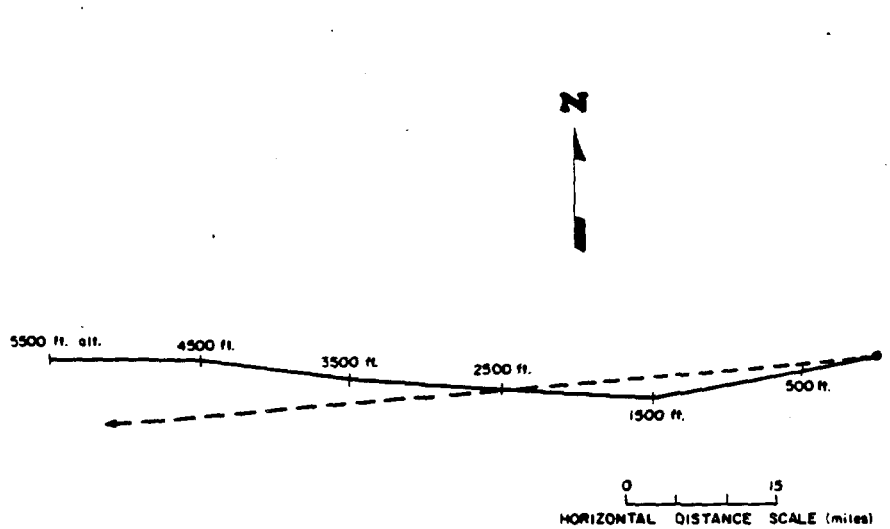

Figure 1.4 Hodograph of wind structure assumed for model calculations. Calculations were made along dashed line. Hodograph is drawn for 1,000-foot-per-hour balloon-rise rate.

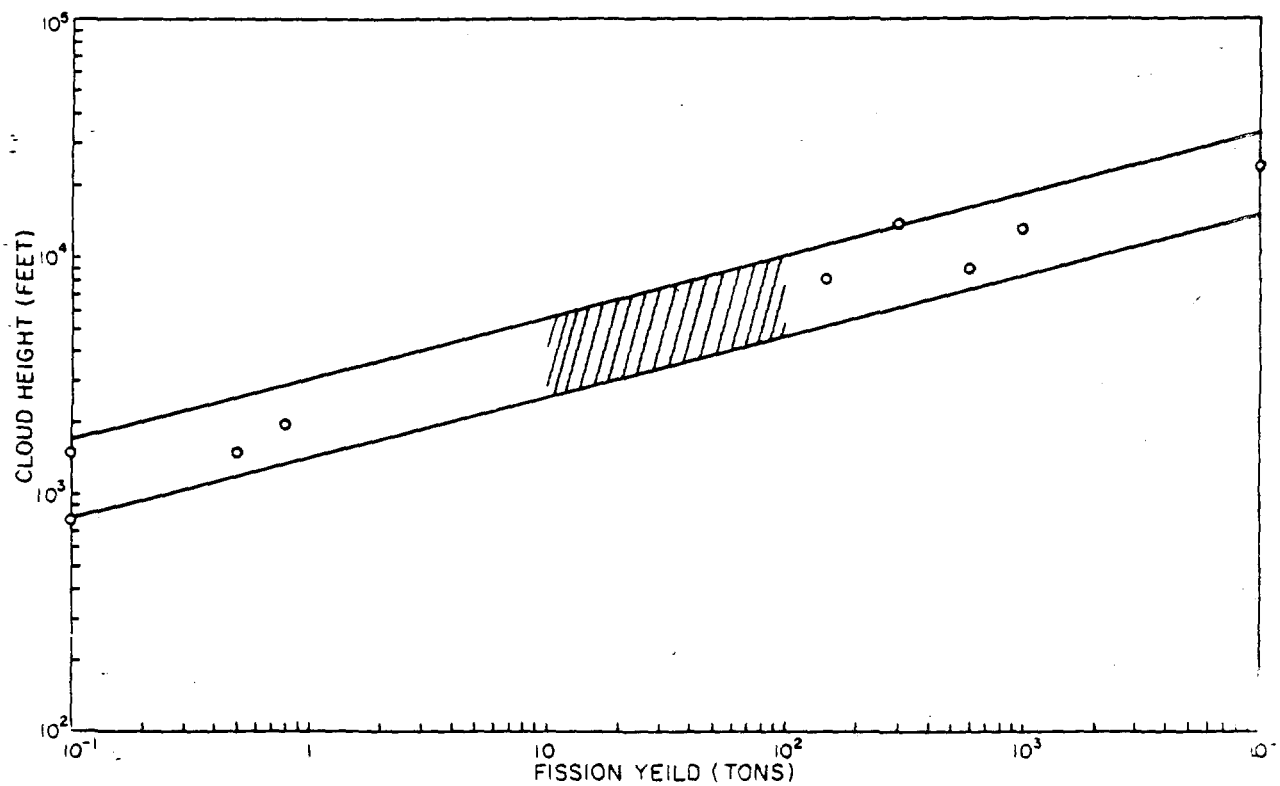

Figure 1.5 Cloud height versus yield.

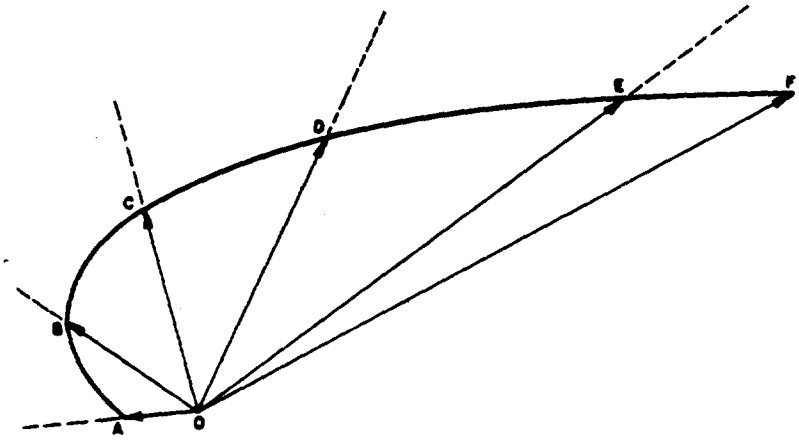

Figure 1.7 Example of a hodograph.

Chapter 2

PROCEDURE

2.1 SPECIAL REQUIREMENTS AND CONDITIONS

2.1.1 Nevada Test Site Soil. Coral soil is neither physically nor chemically similar to other widely occurring soils. Also, essentially all fallout data for yields below the megaton range has come from bursts over NTS soil, which is a more typical soil. To minimize confusion in interpreting fallout results, NTS soil was substituted for coral soil in the expected crater volume and outside the crater over areas that were expected to contribute debris to the cloud. For this purpose, over 130 tons of soil from NTS, Area 10, were used at the Eniwetok Proving Ground (EPG). Figure 2.1 pictures the conically shaped excavation 30 feet in diameter and 8 feet deep that was prepared for placement of NTS soil. This soil was compacted to about 90 percent of its measured natural density of 116 lb/ft^3. NTS soil covered the surface to a radius of 35 feet with a minimum thickness of 6 inches.

2.1.2 Burst Environment. Shot Fig served not only to provide effects measurements but also to test the warhead. Diagnostic measurements of warhead performance required that some equipment be located near the device. This instrumentation together with the standard firing gear used for Operation Hardtack caused the burst environment to be somewhat different from that desired for simulation of surface burst fallout. However, only three pieces of electronic equipment were located within the expected crater radius, with relatively heavy pieces at least 25 feet away. Table 2.1 lists the equipment used, its distance from ground zero, and its mass. Figures 2.2 through 2.4 show the actual preshot arrangement of equipment around the device. To simulate a contact burst of the weapon, the device was detonated on a light wooden stand, which positioned the center of the pit 1 foot above the ground surface.

2.2 INSTRUMENTATION

Scarcity of land areas over which fallout could be measured complicated the instrumentation problem. To estimate the fallout-intensity pattern that would have resulted over an extended land mass, fallout collectors calibrated in terms of full-field dose rates were used for the major part of the instrumentation.

2.2.1 Layout of Instrumentation Array. The instrumentation array was located according to 146 surveyed points comprising one rectangular and one radial grid system. In Figures 2.5 and 2.6 the array is shown superimposed on the maps of Site Yvonne. The stations were identified as indicated in the diagrams. There were 92 lagoon stations, 46 land stations, and 8 reef stations established to carry the array.

2.2.2 Remote Area Monitoring System. Two remote area monitoring systems (RAMS), manufactured by Jordan Electronics, were used in this experiment, one system of 10 units

installed on Site Yvonne and one of 6 units on a YCV barge in the lagoon. A typical remote station is shown in Figure 2.7. Each remote unit consisted of a Neher-White ionization chamber and a remotely operated check source, all mounted in a waterproof housing, 3 inches in diameter by 6 ¼ inches long. Each remote station was hard-wired to a central control station (Figure 2.8). All land units were set on a range of 1 to 1,000 r/hr, except for Stations B-60 and K-65, which were set on a range of 1 to 1,000 mr/hr. Half the units installed on the S-6 barge were on the high range, the others on the low.

Each channel was calibrated prior to D-day, using a 200-mc Co^{60} source for the r/hr range and a 15-mc Co^{60} source for mr/hr range. Maximum field obtained using the stronger source was 10 r/hr. In the laboratory a calibration was made to 1,000 r/hr.

Two sleds with a remote detector mounted on each were to be pulled into the crater at H + 10 minutes (Figure 2.9).

Each RAMS remote station detector was covered with a plastic bag to prevent contamination of the detectors during the fallout. Strings used to tie on the bags at the fixed-field stations were burned off by closing a bridge-wire circuit at the land control station after fallout cessation. Bags covering the sled-mounted detectors were pulled off by the action of hauling the sleds out of the sled shelter.

2.2.3 Portable Survey Instruments. Gamma-dose rate was measured using Jordan AGB-500B-SR and AN/PDR-T1B portable meters. The Jordan instruments contain the same type of ionization chamber as is used in the RAMS. All portable instruments were calibrated using the Rad-Safe calibration range on Site Elmer. Field readings were taken by monitors holding the meters 30 inches above the ground and facing ground zero to minimize body-shielding errors. All 46 land stations were designated as monitoring stations.

2.2.4 Barge Stations. Large flat-topped barges were positioned at five stations in the lagoon to provide collection areas for fallout. Coral soil was spread on the decks of the barges to simulate the effects of soil irregularities on measured dose rates. The soil also prevented formation of rain puddles on deck plates, which could drain away collected fallout particles with postshot rainfall.

Sticky-pan fallout collectors were positioned on the barge decks so that the uniformity of fallout deposition could be investigated. Figures 2.10 and 2.11 show instrumentation layouts for the three types of barges used. Positions of barges in the instrumentation array are indicated in Figure 2.5. An estimate of the fraction of full-field dose at the center of each barge, based on uniform deposition of fallout, is given in Table 2.2.

2.2.5 Fallout Collectors, Sticky Pans. Sticky-pan fallout collectors consisting of 8- by 10-inch flat metal trays covered with an alkyd-resin toluene solution and mounted on 2-foot-square baffle plates were used for collecting fallout data.

Seventy-two fallout collectors were installed at 32 stations ashore. A typical installation is shown in Figure 2.12.

For stations in the lagoon where water depth ranges from 15 to 200 feet, collectors were mounted on small buoys. At 87 lagoon stations a single buoy-mounted fallout collector provided the only instrumentation. One such station is shown in Figure 2.13.

Eight fallout-collector stations were installed on the reef upwind from ground zero. Baffle plates were mounted about 5 feet above low-tide level so that they would be approximately 30 inches above high-tide level.

Clusters of sticky-pan fallout collectors were established at various locations in the array to determine the statistical spread in sticky-pan readings, to examine the effects of weathering on pans that could not be collected before being exposed to rain, and to calibrate

sticky-pan data in terms of equivalent full-field dose rate. Six collectors were used per cluster. For studies of weathering effects, it was planned to collect three pans of some clusters as soon after the shot as possible and to collect the remaining three when recovery of other pans in the same portion of the array was complete. When clusters were used for statistical studies alone, all six pans were collected at the same time.

2.2.6 Sticky-Pan Counting. Instrumentation for measuring the amount of gamma activity collected on sticky pans was installed in a tent near Station 1520 on Yvonne. The primary equipment consisted of two geometries. Each geometry included four GM tubes and a scaler to measure count rate. Five shelf positions in the geometry allowed pans to be placed at different distances from the tubes. One of these geometries is shown in Figure 2.14. As a secondary measurement method, mainly for counting activity too intense for the first method, a geometry mounting a Jordan AGB-500B-SR gamma meter was used.

2.2.7 Air Samplers. One high-volume (50 cfm) air sampler was installed on each of the smaller barges, and two were installed on the large barge. Each sampler used a 4-inch-diameter GM-2133 filter. The intake airspeed of 8 knots was expected to nearly match the surface windspeed during the sampling period. Air samplers were alined to face into the prevailing wind. Figure 2.15 shows an air sampler station.

2.3 OPERATIONS PLAN

2.3.1 Weather Requirements. The limited amount of instrumentation available for measurement of fallout in the lagoon was placed in an array oriented for the prevailing wind direction, $\pm 10°$. It was required that winds at shot time have the proper direction to assure that the fallout pattern would not miss the array. Windspeeds were restricted to 20 knots or less to assure that a reasonable percentage of activity would be sampled. Project 34.10 provided the preshot wind data necessary for the H-hour precision.

Additional requirements were that there be no rain for at least 2 hours postshot and that no cloud cover that would interfere with balloon tracking and shot-cloud photography.

2.3.2 Remote Area Monitoring System. The two RAMS were activated by H−1 hour and operated continuously until the dose rates had fallen below significant levels. RAMS station operators transmitted readings periodically to the control point at Station 1520 to permit early calculations of the fallout phenomena. The sled-mounted RAMS were pulled into the crater by H + 10 minutes.

2.3.3 Land Recovery Parties. Land recovery parties entered the field starting at H + ½ hour. Reentries were made thereafter at a rate calculated to secure complete data at the earliest possible time without overexposing available personnel. Each recovery party comprised at least one project monitor and one Rad-Safe monitor. A simple procedure was developed to permit early recoveries with a high probability that personnel would not receive more than an allowable radiation exposure dose. The procedure required controlling the total time spent by a party in the field and limiting penetration to fields of less than a maximum dose rate. Dose rate was determined by the time required to perform a recovery mission and the available dose (that dose which each person in a party may receive and not exceed AEC tolerances).

Each recovery party was assigned a maximum time required for a specific recovery mission. With the available dose known, Table 2.3 was used to find the maximum-dose-rate field that a party was allowed to enter. Personnel would proceed directly into the

field until the maximum dose rate was reached or until slightly less than half of the assigned time had elapsed for short recoveries. They would then return toward the starting point, recovering sticky pans and monitoring until maximum time allowed in the field had elapsed. Back at the starting point, dosimeters were read, a new and smaller allowable dose calculated, and a new recovery entry planned.

2.3.4 Lagoon Recovery Parties. Five LCM's boats and one DUKW were used by the lagoon recovery parties in collecting buoy sticky pans. A water taxi was used to transport personnel to the barges. All parties entered the fallout field by H + ½ hour.

2.3.5 Sticky-Pan Counting. Sticky pans collected from the fallout field were brought to the counting tent at Station 1520 by helicopter, water taxi, LCM, DUKW, weapon carrier, and jeep. Pans were laid out on a large concrete pad marked with the same coordinates as used in the field and were systematically brought into the tent for counting throughout D-day, that night, and D + 1.

2.4 REQUIRED DATA

2.4.1 Full-Field Dose-Rate Calibration. The original plan for calibration of sticky-pan data in terms of full-field dose rates was as follows: Recordings of full-field dose rate versus time from each of the fixed RAMS stations on land were to be associated with graphs of average count rate versus time for the sticky-pan cluster at each of the stations. The full-field dose rate corresponding to any sticky-pan count at any time could then be determined. To minimize the effect of fractionation and collection efficiency that might depend upon location in the fallout field, calibration obtained from a given RAMS station was to be applied only to sticky pans collected from nearby stations.

A similar procedure was to be used to calibrate buoy sticky pans. In this case, the average of the readings from the cluster in front of each barge was to be compared with dose-rate readings at the center of the respective barge. Dose-rate readings were corrected to full-field readings, where a uniform deposition of fallout on the barge was assumed. Corrections for nonuniformity could then be made from barge sticky-pan data.

The ratio of the dose rate measured with a survey instrument at a sticky-pan station near the shoreline to the full-field dose rate indicated by the sticky-pan count at the same H-plus time would then be a measure of the fraction of full field at that location and could be used to correct other survey readings taken at comparable locations. Because of developments that could not be anticipated, several changes were made in the calibration procedure. These changes are discussed in the next chapter.

2.4.2 Air Samplers. Filters from the air samplers were counted in the same geometry used for sticky-pan counting. By relating the count rates of filters and adjacent survey meter and sticky-pan readings, an estimate of the contaminant mean fall rate was obtained by using Equation 1.5.

2.4.3 Wind Measurements. Winds were measured by manual tracking of free-rising balloons with two Signal Corps PH-BF33 Akeley phototheodolites. Locations of the phototheodolite stations and the remotely controlled balloon release stations are shown in Figure 2.16.

2.4.4 Cloud Dimensions. Cloud photographs were obtained from three camera stations located at positions shown in Figure 2.17. Stations on Wilma and Elmer were atop 75- and

100-foot towers. The station on the shot island of Yvonne was established on top of a concrete shelter designated Station 1520. Facts concerning the cameras used are summarized in Table 2.4.

2.4.5 Plutonium Contamination Survey. A limited survey for plutonium contamination and sample collection for later analysis was required to establish a correlation between plutonium and fission-product fallout.

TABLE 2.1 BURST ENVIRONMENT

The following lists the mass of the different items located at Shot Fig ground zero. The mass was determined by estimating or by weighing the individual item when possible.

Description of Instrument	Distance from GZ	Weight
	feet	lb
Canvas ground cover	0 to 8	25
Cables	0 to 20	30
Beryllium	1	8
Quint and P.C.	2	60
P.C. stand	3	2
Zippers	3	38
X Unit	20	18
Paraffin	1	70
Zipper detector	3	30
Duplex outlets	10	6
Vacuum pump	12	40
Zero rack, including battery charger and batteries	20	740
Zero rack cabinet	20	167
Telemetering transmitter	20	65
Telemetering transmitter cabinet	20	82
Power panel	20	25
Power panel board	20	28
Breaker panel	20	10
Signal panel	20	3
Signal panel board	20	8
Radio antenna	25	6
Telemetering transmitter antenna	30	10
Telemetering transmitter mast	30	47
Tent	8 to 25	1,390

TABLE 2.2 FRACTION OF FULL-FIELD DOSE RATES, BARGES

Type of Barge	Dimensions	Fraction of Full-Field Dose Rate
	ft	
YCV	60 × 200	0.52
YC	32 × 100	0.38
Sectional	30 × 60	0.35

Table 2.3 RECOVERY PARTY PARAMETERS

Available Dose	Maximum Time	Maximum Rate
r	min	r/hr
3	5	36
	10	18
	15	12
2	5	24
	10	12
	15	8
1	5	12
	10	6
	15	4
	30	2
	60	1

TABLE 2.4 TYPES AND LOCATIONS OF CAMERAS

Number	Camera Type	Focal Length Lens	Location	Operating Speed	Field of View	
					Width	Height
		mm		frames/sec	ft	ft
1	35-mm Automax	28	Yvonne	1	3,180	3,180
2	35-mm Varitron	90	Yvonne	1	2,180	1,510
1	Graphic (4 × 5)	90	Yvonne	Manual	5,790	5,040
1	70-mm EG&G	105	Wilma	2	8,640	12,800
1	35-mm Automax	28	Wilma	1	11,880	11,880
1	70-mm EG&G	305	Elmer	2	8,000	12,500

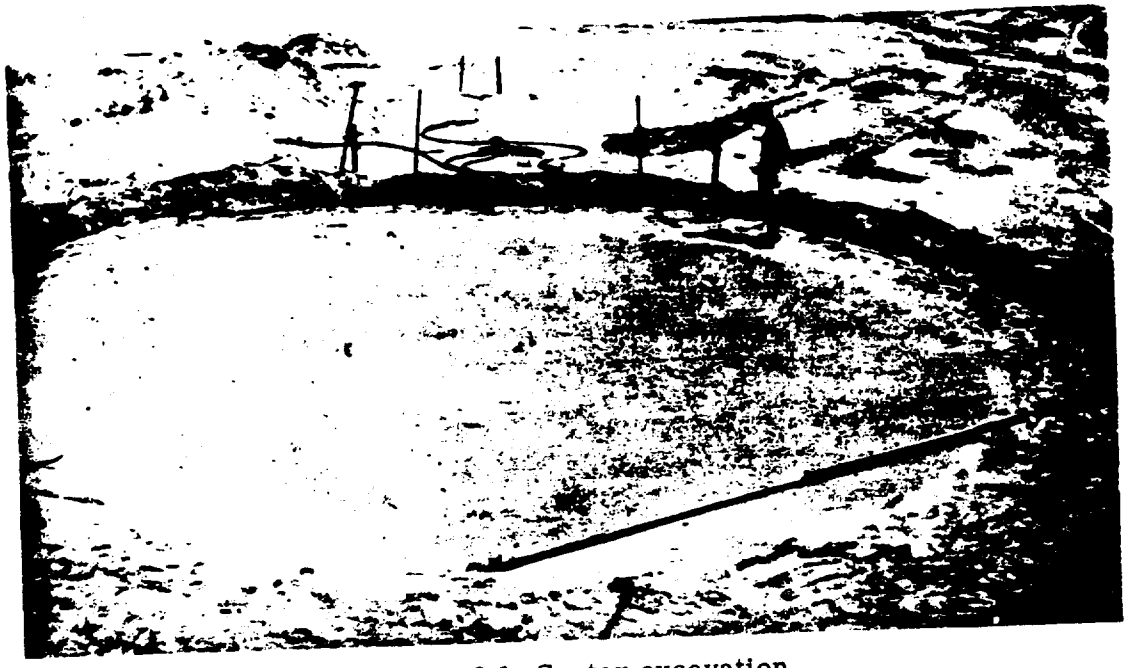

Figure 2.1 Crater excavation.

Page 27 deleted.

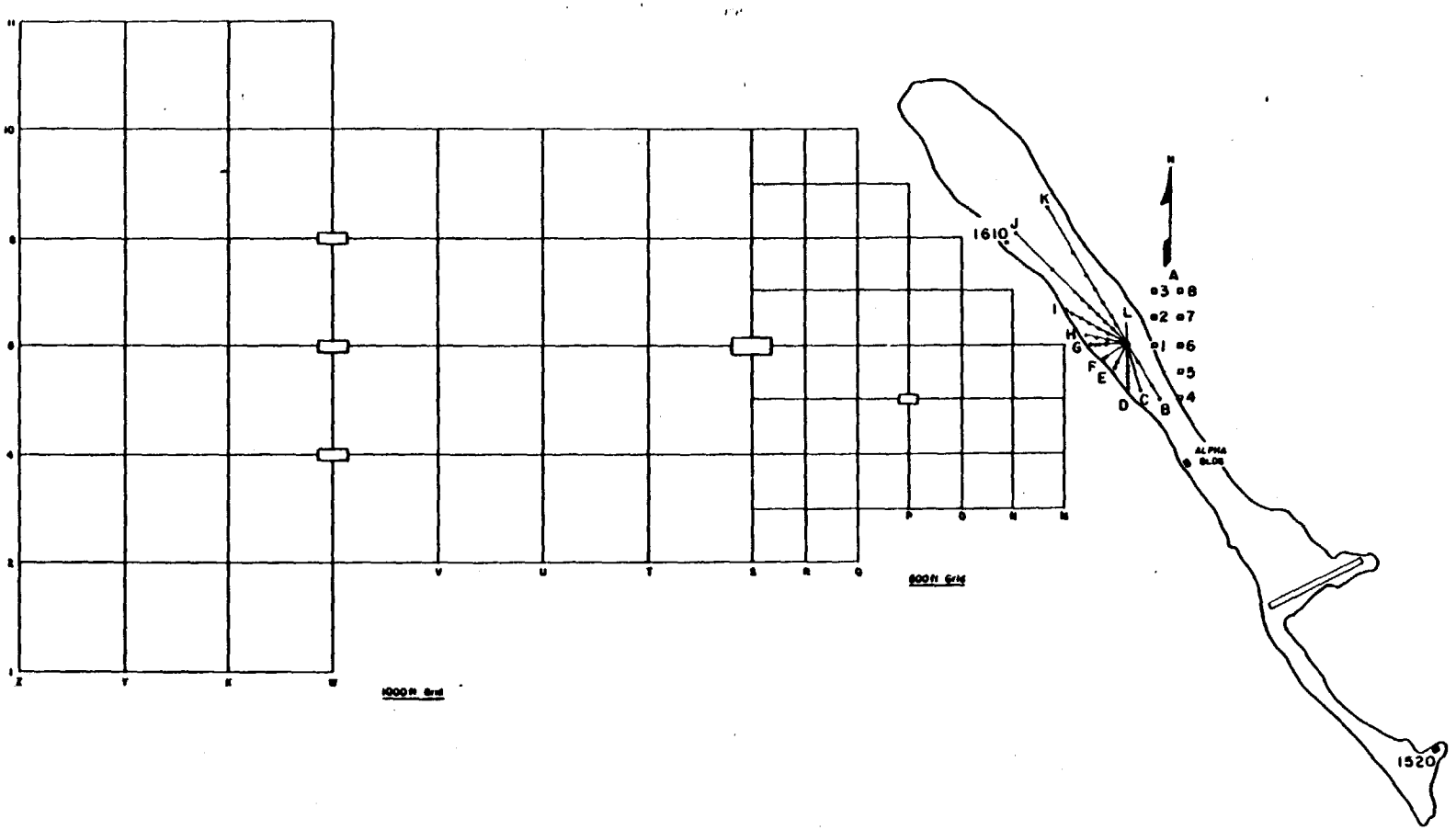

Figure 2.5 Instrumentation layout, lagoon.

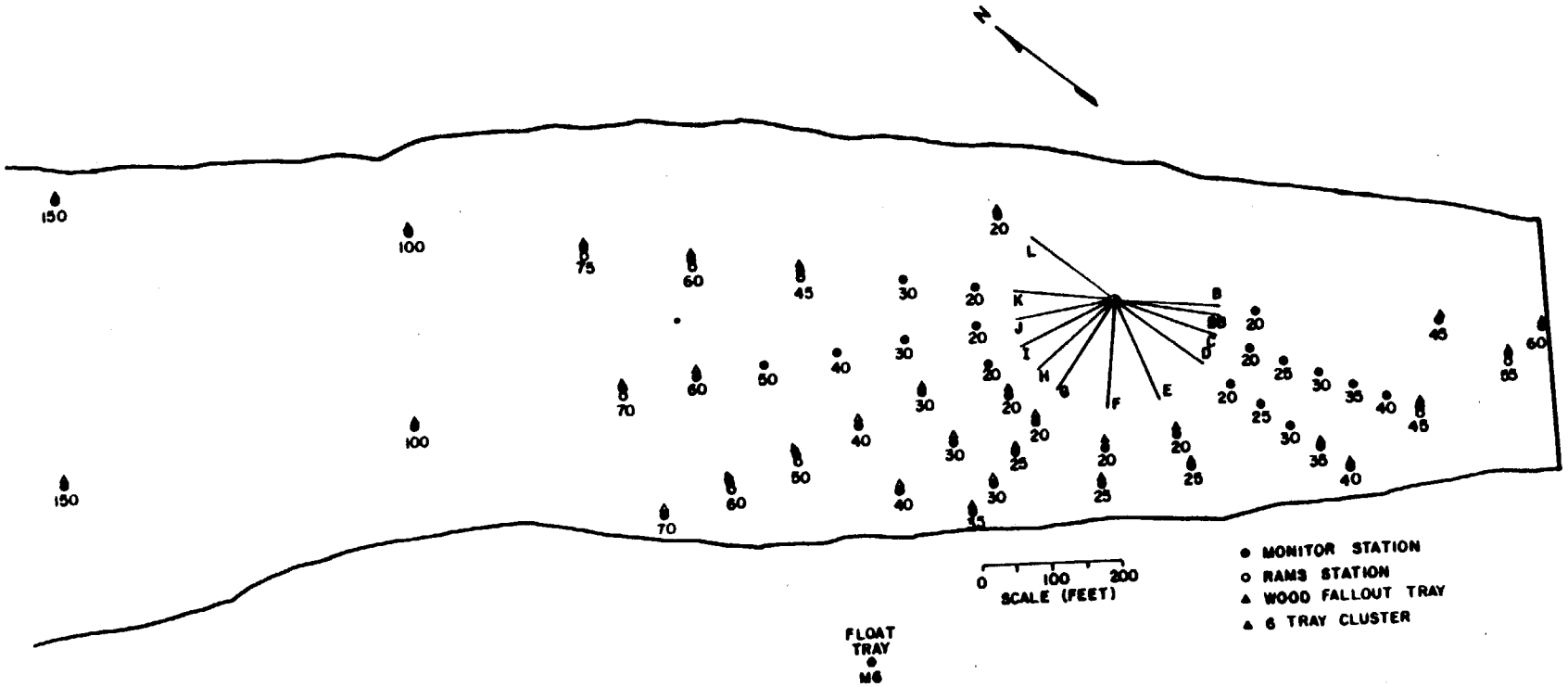

Figure 2.6 Instrumentation layout, land.

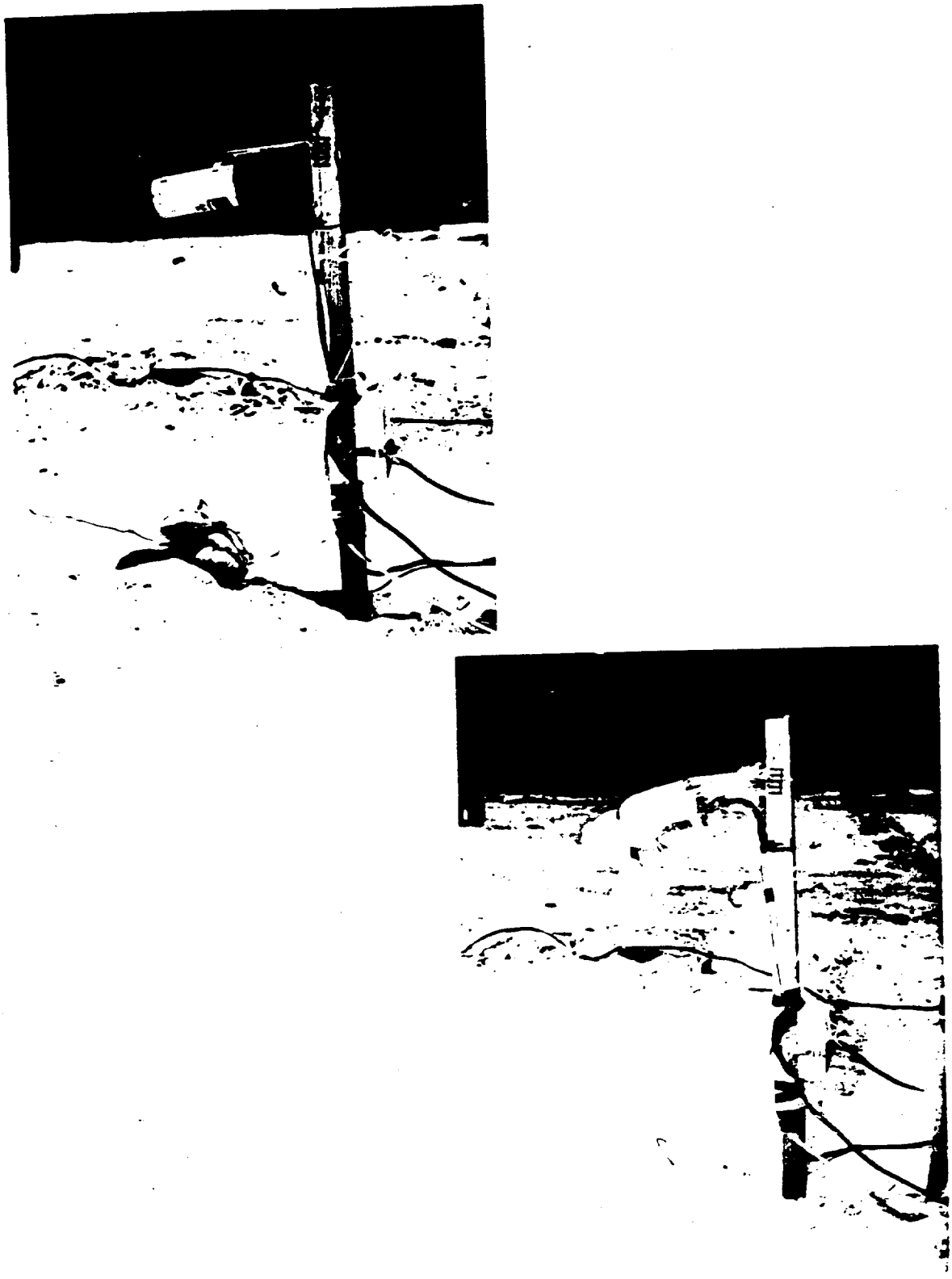

Figure 2.7 RAMS detectors, land stations.

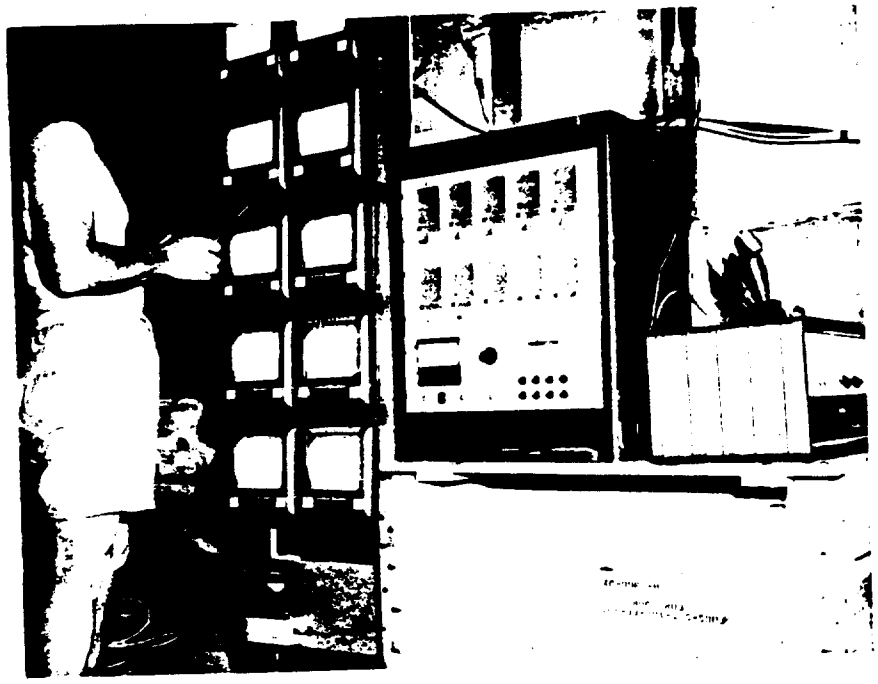

Figure 2.8 RAMS control station.

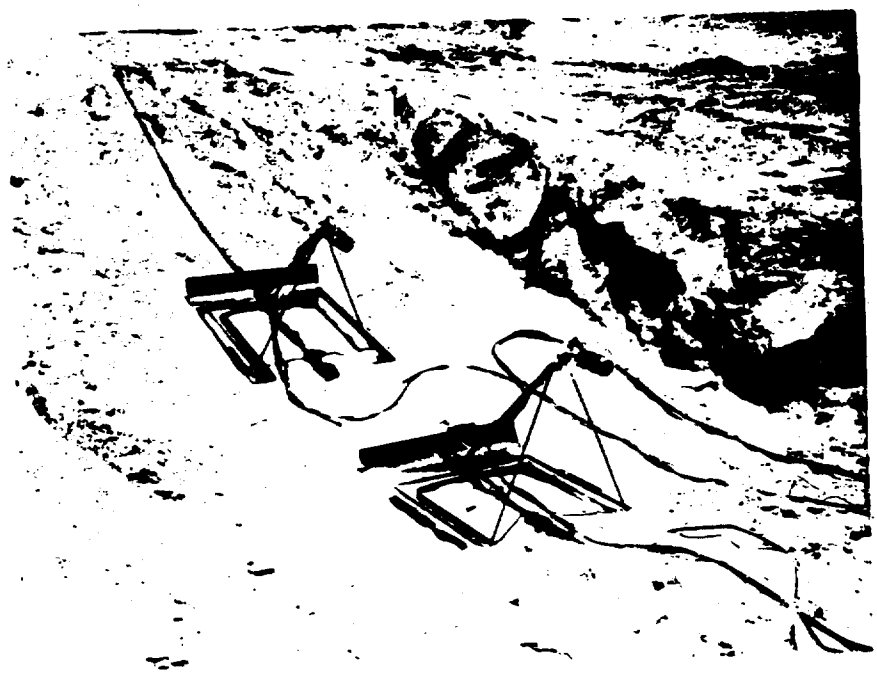

Figure 2.9 RAMS detectors on sleds in blast shelter prior to H hour.

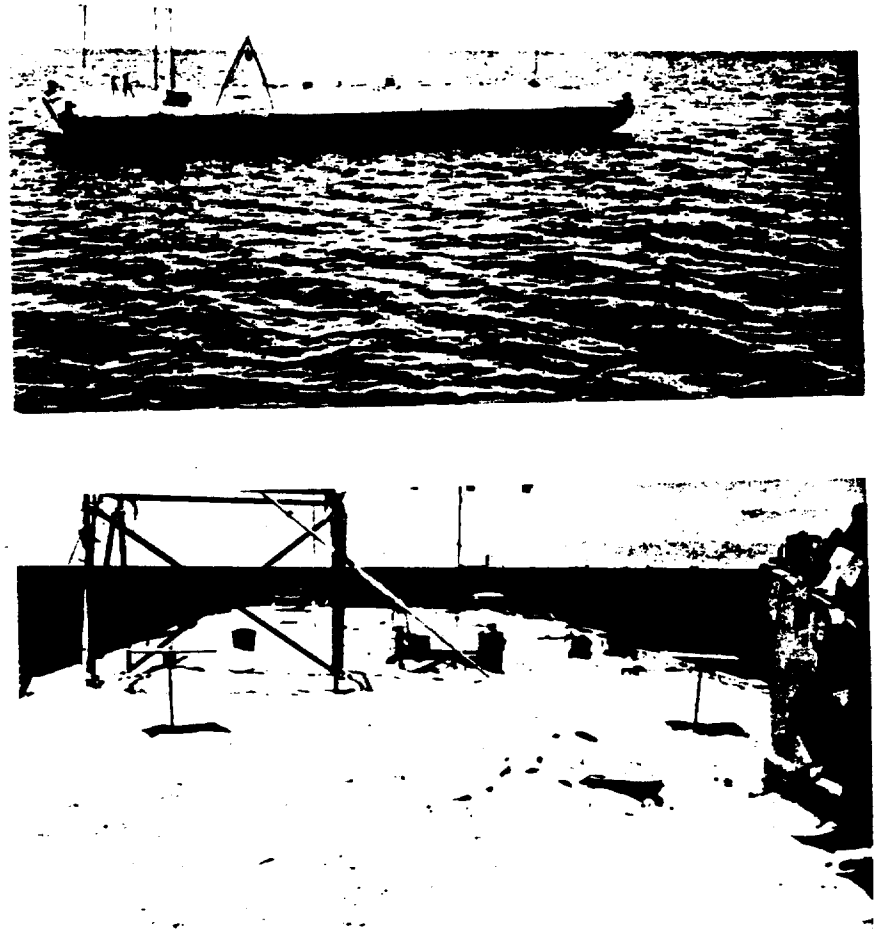

Figure 2.10 Barge instrumentation.

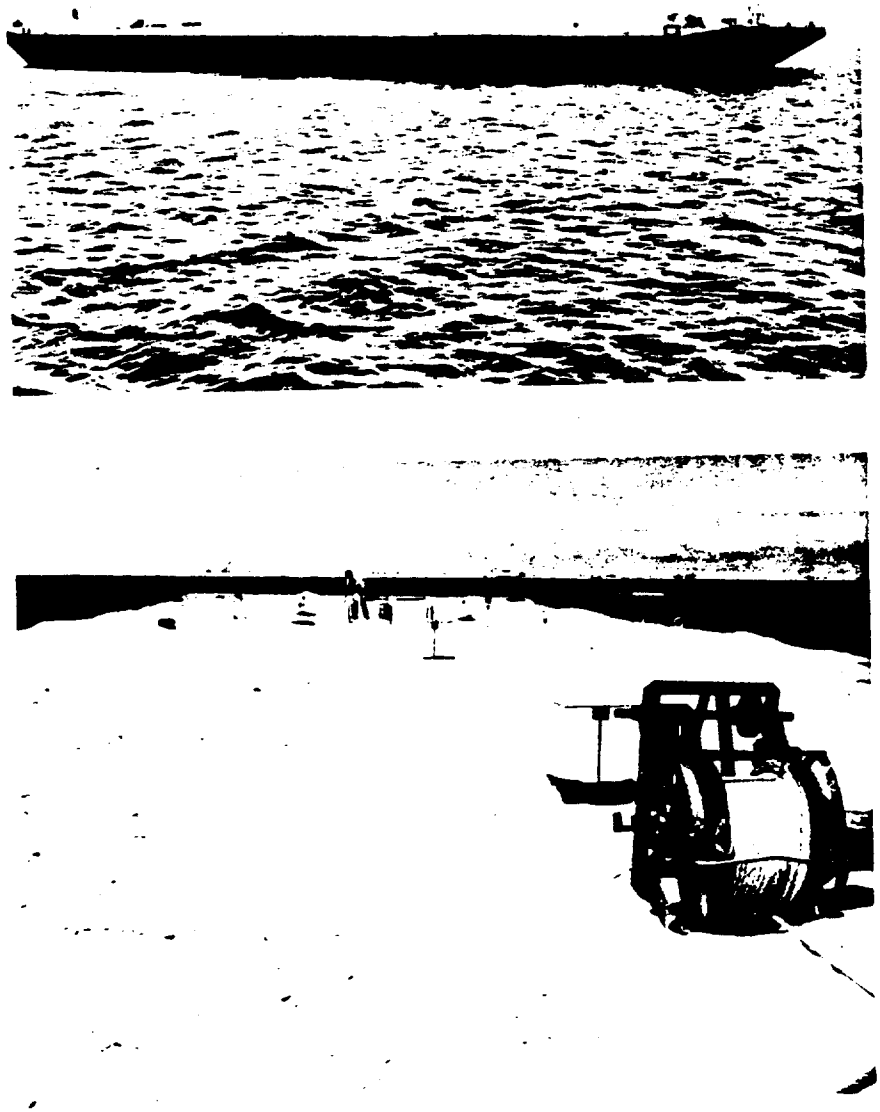

Figure 2.11 Additional view of barge instrumentation.

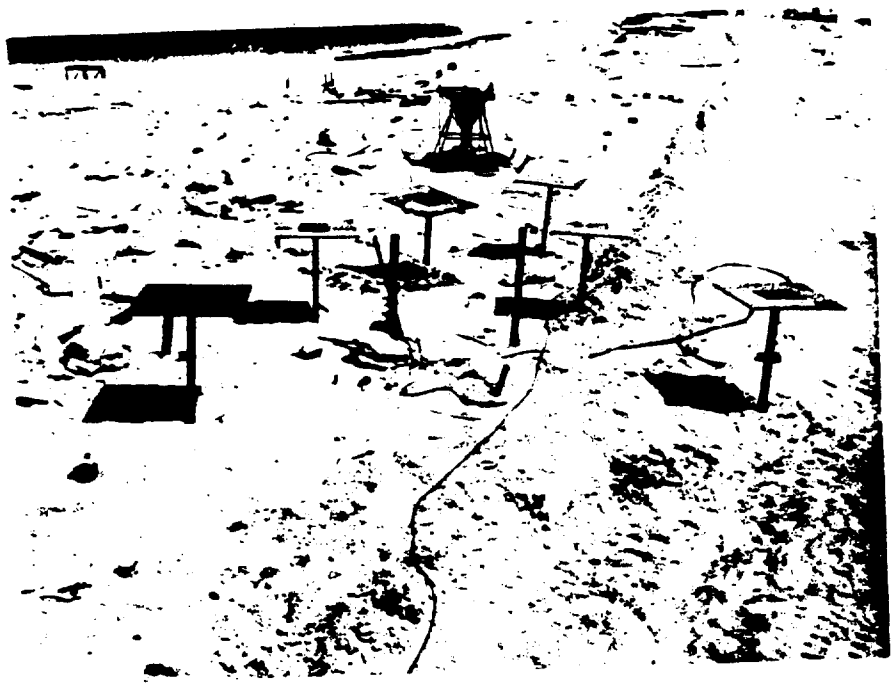

Figure 2.12 Fallout collectors, land.

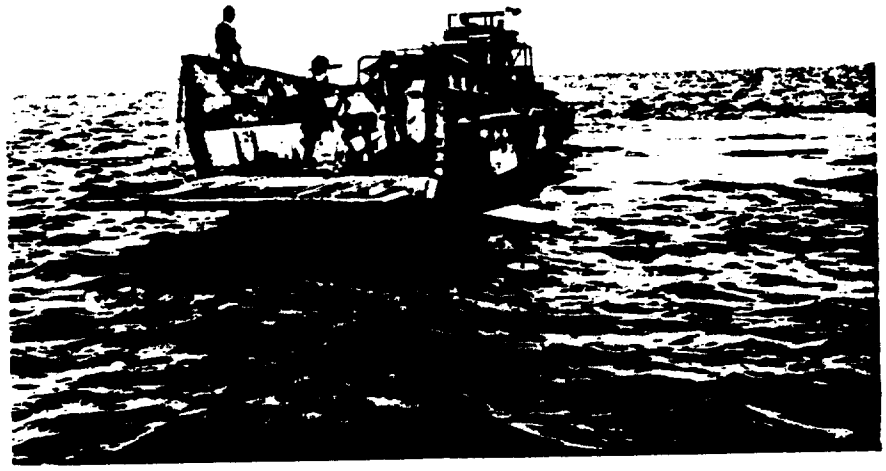

Figure 2.13 Fallout collector, buoy.

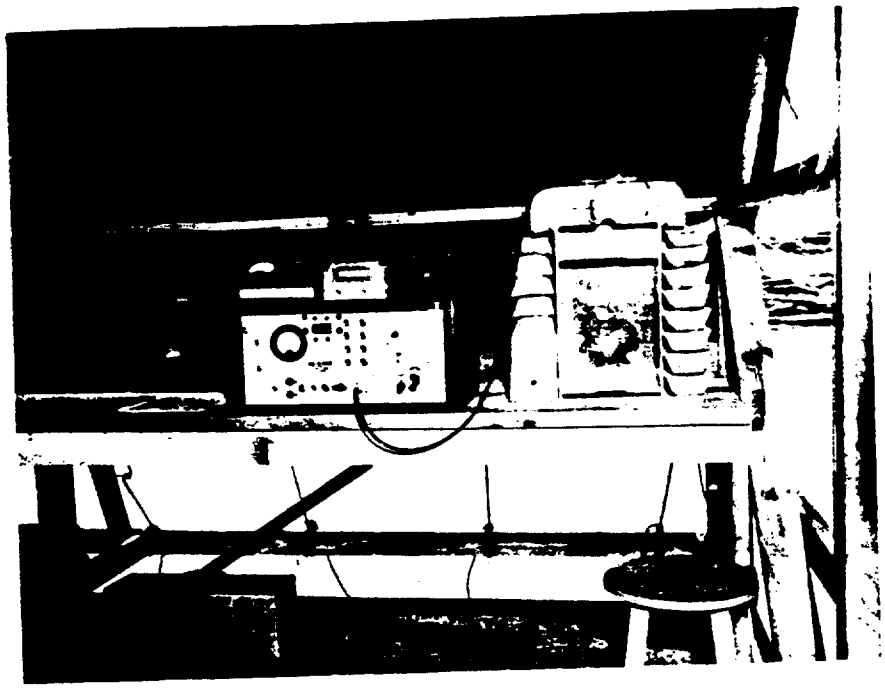

Figure 2.14 Counting geometry.

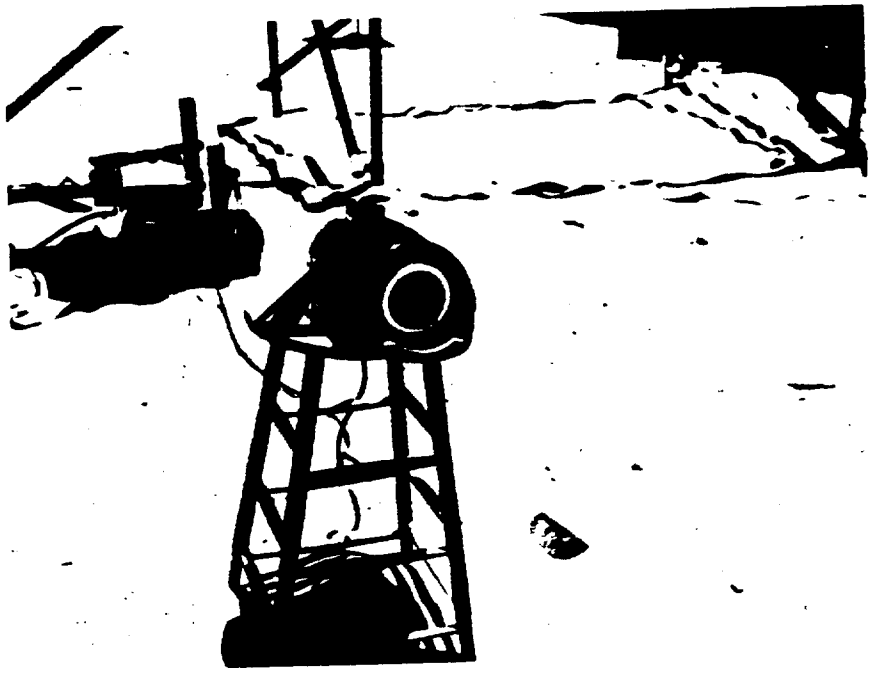

Figure 2.15 Air sampler on a barge.

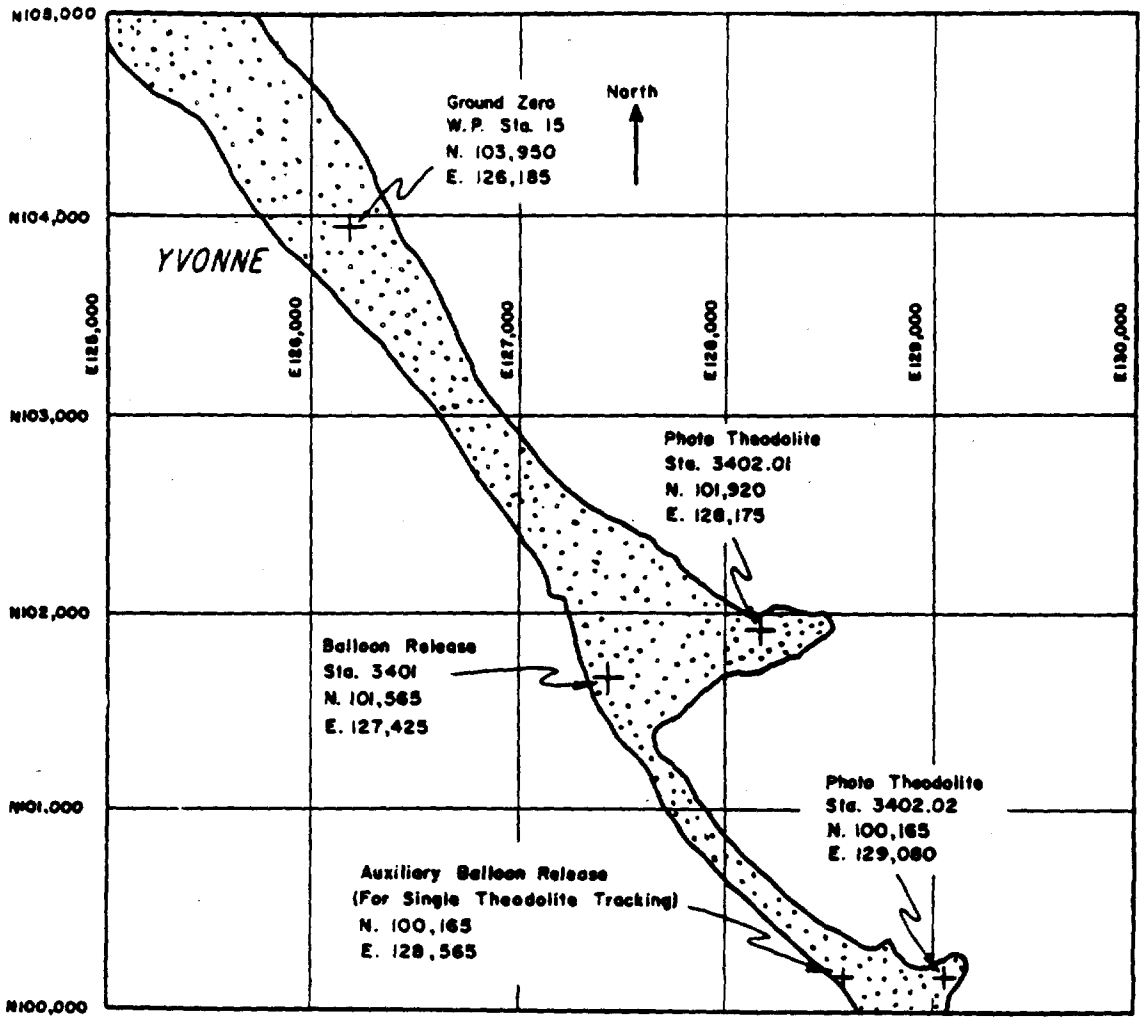

Figure 2.16 Phototheodolite and balloon release locations.

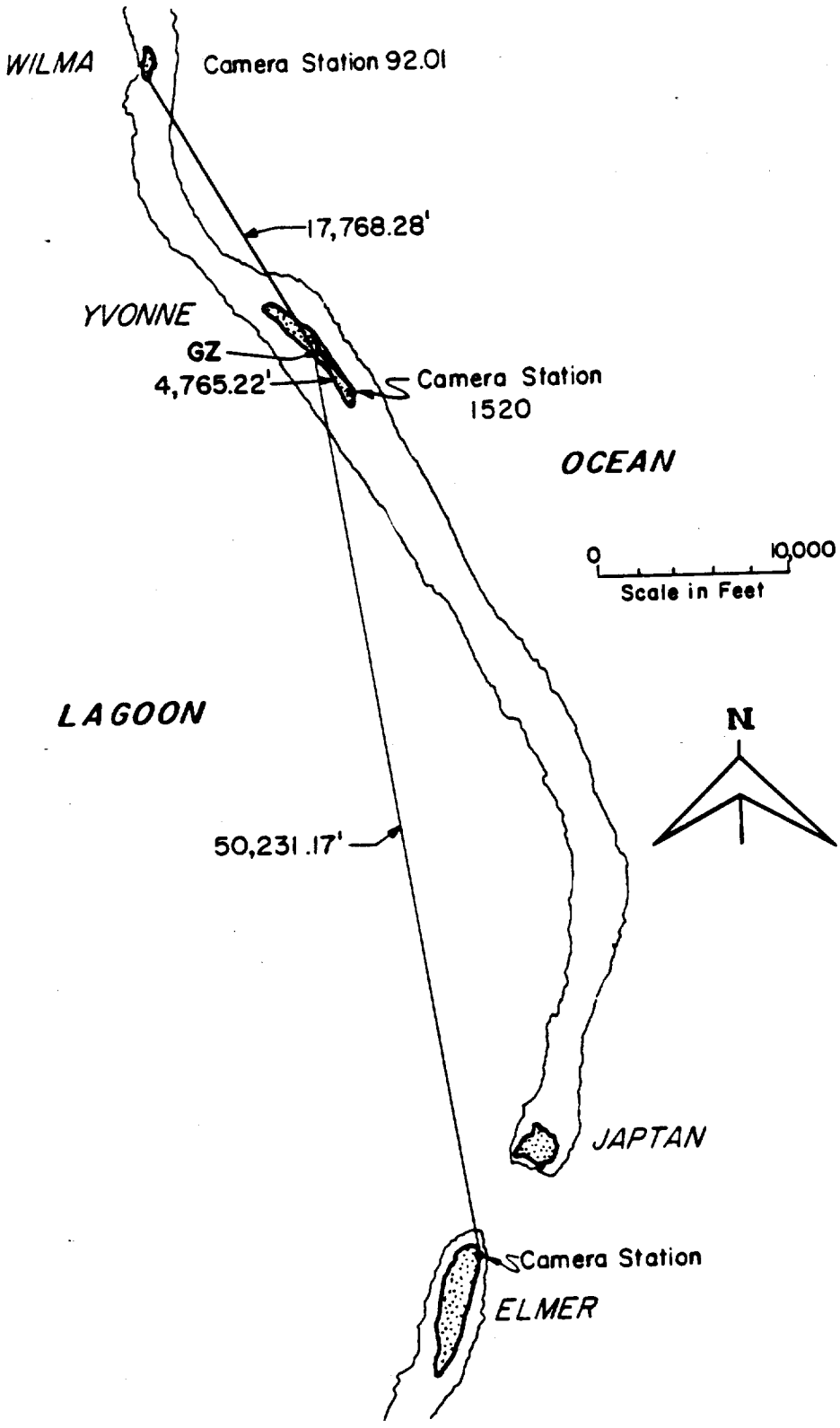

Figure 2.17 Layout of camera stations.

Chapter 3

RESULTS AND DISCUSSION

3.1 EFFECT OF THE DELAY BETWEEN SHOTS QUINCE AND FIG

The original plan was to make this fallout study during Shot Quince, 6 August 1958. it was decided to use the same instrumentation array to measure fallout from Shot Fig.

Shot Fig occurred 18 August at the same ground zero that was used for Quince. During the time between shots, the buoy collector array suffered extensive damage due to high winds and heavy seas. Although replacement buoys were manufactured from available material at EPG, they were not as rugged as the originals, and by 18 August one-third of the buoy stations were missing. In addition, three buoy clusters were reduced from six to three collectors; the remaining two clusters had only a single buoy each.

3.2 FISSION PRODUCT SOURCE STRENGTH

Relating to the gamma source strength of fission products at the reference time of 1 hour after zero time (H + 1 hour), the following will be assumed: (1) For 1 kt of fission products, the gamma source strength is 5.8×10^{22} Mev/hr. (2) For uniform distribution of 1 kt of fission products on an area of 1 mi^2, a dose rate of 2,650 r/hr will be recorded by instruments at a height of 3 feet above the ground surface.

References 4 and 5 provide the basis for these numbers and show that the well-known $t^{-1.2}$ decay approximation may be expected to apply reasonably well for the time period of 1 minute to a few thousand hours after zero time. That is, during this time period, a dose calculated from a measured dose rate and the $t^{-1.2}$ decay approximation would be expected to differ from the actual dose delivered by no more than 50 percent, provided fractionation effects are not more important than estimated in Reference 5 and discounting the importance of weathering or translocation of debris by wind erosion.

3.3 CLOUD DEVELOPMENT

The Speed Graphic camera on Yvonne was intended to be the primary instrumentation for cloud dimension data. However, low cumulus clouds partially obscured the detonation cloud from the Yvonne station, making it difficult to obtain complete measurements after H + 4 minutes. The Wilma station served to provide the bulk of data for cloud dimensions. Figure 3.1 shows a schematic of cloud development drawn from observations taken on Wilma. The double-puff shape was also observed on the surface detonation of Operation Jangle and may be an expected feature for a surface burst cloud.

Dimensions for general features of the cloud are indicated in Figure 3.2 by Diameters A, B, and C, and by Heights h_1, h_2, and h_3. Figures 3.3 and 3.4 show the values of these

dimensions as a function of time. Corrections for cloud drift have been applied by using wind measurements to plot the cloud trajectory.

The top of the cloud had not reached its maximum height by the time it had drifted beyond the instrumentation array 7 to 8 minutes after the detonation.

3.4 WINDS DURING FALLOUT DEPOSITION

Shot Fig occurred at 1600 hours, after several hours' delay caused by unfavorable wind directions.

Single-theodolite balloon trackings were made at H−20, H−10, and H+3 minutes. To infer hodographs from the data, it was necessary to assume either a known rise rate for the balloon or known windspeeds. Experience gained on earlier double-theodolite trackings during the day indicated that it would be best to assume known windspeed. Hodographs for these three balloon releases are shown in Figure 3.5. Relatively large errors are possible in range and elevation for these three hodographs; however, bearings are accurate to ±0.001 radian.

Also shown in Figure 3.5 is a hodograph taken from the double-theodolite balloon tracking which started at H+9 minutes. This must be taken as the best description of winds that existed during fallout deposition. However, some idea of variability with time is indicated by the composite of Figure 3.5.

Balloon rise rates varied on these balloon runs, but all have been adjusted or normalized to a rise rate of 1,000 ft/min. All of the hodographs have been superimposed on ground zero for Shot Fig to show their orientation with respect to the instrumentation array. Results show that wind directions were ideal for fallout sampling. Windspeeds measured at H+9 minutes varied from 11 knots for the layer from the surface to 250 feet altitude to 16 knots for the layer from the surface to 5,000 feet.

Balloon runs at H+3 and H+9 minutes were recorded on film in addition to being recorded manually.

3.5 MEASURED FALLOUT

3.5.1 Land Areas. Dose rates for all land stations at the reference time of 1 hour after detonation are shown in Figure 3.6. These values were taken entirely from monitor readings made with Jordan survey meters. Survey meter readings were used in preference to RAMS data for the land stations, since the RAMS land equipment was damaged by an electrical transient produced by the nuclear detonation. In most cases, dose-rate values were determined by more than one reading (sometimes as many as seven) during the period from H+35 minutes to H+50 hours. For a given location, all readings were adjusted to the reference time of H+1 hour, assuming $t^{-1.2}$ decay. An average of these H+1 hour dose rates was computed and is the value shown for each station in Figure 3.6. Correction factors have been applied in those cases where the monitor stations were located near or on the shoreline. These factors were never greater than 1.5.

Table 3.1 was constructed to give some idea of the relevance of the $t^{-1.2}$ decay assumption to actual observations in the field. For each station location where three or more readings were obtained, the number of readings is listed together with the time interval (measured after zero time) during which the readings were taken. The fourth column is the minimum percentage error that can be assigned to each dose-rate measurement in order for all measurements made during the interval to be consistent with the $t^{-1.2}$ decay rate. For about 60 percent of the stations, errors smaller than ±30 percent in dose-rate measurement could, by themselves, explain apparent deviations from $t^{-1.2}$ decay. The very

large inconsistency indicated for the crater lip measurements could have been cuased in part by a cave-in of crater walls caused by postshot rain.

3.5.2 Lagoon and Reef Areas. The plan to establish a calibration of buoy-mounted sticky pans by comparing dose rates measured on the large barges to counting rates of nearby buoy-mounted sticky pans had to be abandoned when large numbers of the buoys were lost. Instead, land measurements were used to establish a calibration that was assumed to apply everywhere in the fallout area.

At 16 land stations where H + 1 hour dose rates were obtained, sticky-pan fallout collectors were recovered and counted. A composite sticky-pan decay curve (Figure 3.7) was obtained from four of these and from three buoy-mounted sticky pans. All pan counting rates were normalized to H + 3 hours by use of this composite decay curve.

The ratio of H + 3 hours count rate to H + 1 hour dose rate was found for each of the 16 land stations; the mean ratio was determined from the graph shown in Figure 3.8. The mean ratio was used to determine full-field dose-rate estimates for lagoon and reef stations. It was also determined from this curve that ± 50 percent is the probable error for a dose rate inferred by a single, land sticky-pan reading. Table 3.2 lists counting and dose rates.

3.5.3 H + 1 Hour Dose Rates for Complete Array. In Figure 3.9, the H + 1 hour dose rates inferred from sticky-pan collectors and from RAMS and monitor readings on the barges are listed for all stations in the lagoon and on the reef. Also shown are intensity contours for the entire array, which represent the best estimate of the H + 1 hour values.

The zero intensity contour was positioned on the basis of cloud trajectory calculations and measured cloud dimensions.

Consistent dose-rate histories were obtained on the YCV barge (S-6) by continuously recording RAMS and by monitors equipped with survey meters. The position of the 1-r/hr contour on the small barge (P-5) is well established from survey data. On both of these barges, readings taken at the center were about the same as readings taken near the edge, indicating uniform deposition of fallout.

Reliable land readings established a hot-line direction on land, which is consistent with cloud trajectory, cloud height, and wind data. The land hot line is directed toward the small barge, showing that contamination came primarily from the 0- to 500-foot altitude range. Hot lines for contamination that fell from higher altitudes up to 2,700 feet passed to the north of the small barge with the 2,700-foot hot line falling on the YCV barge. Data from the 10 buoy collectors (S through M on lines 5 and 6), which covered the important region between these two barges, allow some confidence in the estimated contour lines, especially in the 1-r/hr contour.

3.6 CLOUD SHINE

The RAMS instrumentation that was located on the YCV barge recorded gamma radiation "shine" from the passing cloud. Peak dose rates of 125 and 165 r/hr were recorded by two detectors that were set to cover the 1- to 1,000-r/hr range. Dose rate versus time is shown for these recorders in Figure 3.10. Peak dose rate was observed at slightly less than H + 2.5 minutes.

Calculations of the cloud trajectory, using measured nonuniform rise rate and measured winds, show that the center of the puff passed almost directly over the barge at about 2.4 minutes after zero time. In Figure 3.11, the plan position of that portion of the cloud

between altitudes h_1 and h_2, as shown in Figure 3.1, is superimposed on the instrumentation array for 0.5, 1, 2, 3, 4, and 5 minutes after zero time. The midpoint altitude $(h_1 + h_2)/2$, is given for each of these times.

This, fortunately, not only serves as confirmation of windspeed and direction estimates for the fallout period, but also allows some rough assessment of vertical activity distribution within the cloud.

For the source strength of fission products at 2.4 minutes, Reference 4 gives a value for the Shot Fig debris at H + 2.4 minutes, assuming 1.45×10^{23} fis/kt.

It will be assumed that dose rate as a function of distance from a point source in air can be described with fair accuracy by

$$I = \frac{S}{R^2} e^{-R/320}$$

Where: I = dose rate, r/hr
R = range, meters
S = a constant that is proportional to source strength

If all the fission products from Shot Fig were concentrated at a single point directly over the YCV barge at 2.4 minutes, the height of the point source necessary to produce the average measured dose rate of computed from the above is Reference to Figure 3.4 shows that, at 2.4 minutes about the midpoint for the lower of the two puffs that made up the visible cloud (see also Figure 3.2). This result indicates that the lower part of the visible cloud contained the bulk of the activity.

3.7 CRATER DATA

The two RAMS detectors that were pulled into the crater at H + 10 minutes were apparently damaged by an electrical transient phenomenon and failed at zero time. However, dose rates near and within the crater lip were recorded at plus 3.5, plus 18, and plus 47 hours. Results are shown in Figure 3.12. The crater appeared to be contained within the NTS soil.

A survey was made of the Fig crater on 21 August (D + 3 days). Results are summarized in Figure 3.13. The ledge shown about 4 feet below the crater lip was caused by a cave-in, which may have been the result of postshot rain.

3.8 PLUTONIUM CONTAMINATION

Several sticky pans were returned to Sandia Laboratory for plutonium analysis by radiochemistry. In Table 3.3, results are listed together with gamma dose rates that were inferred by gamma-counting the same pans. The ratio of the two results is also shown. The indication is that gamma dose-rate measurement is a poor way to estimate plutonium contamination at a given location. If there were no fractionation between fission products and plutonium, the ratio would be expected to be about 0.06 r/hr/μgm/m^2. Most of the ratios are very much higher than this, indicating a larger particle size for fission products than

for plutonium. This result is not consistent with results obtained from a one-point detonation where gamma dose rates gave a fair indication of the plutonium present (Reference 3).

Plutonium concentration contours cannot be inferred on the basis of this small amount of data.

3.9 FALL-RATE MEASUREMENTS

Filters from air samplers located on barges in the lagoon were counted in the same geometry used for sticky-pan counting. Results are listed in Table 3.4 together with the mean fall rates that were inferred, where possible, from Equation 1.5. Since the air-sampling rate was 50 cfm and the area of a sticky pan was 0.55 ft^2, the forms of Equation 1.5 used for the calculations were

$$\bar{f} = 90 \frac{C_S}{C_F} \text{ ft/min}$$

and

$$\bar{f} = 1{,}125 \frac{r}{C_F} \text{ ft/min}$$

Where: C_S = average counting rate at H + 3 hours for sticky pans that were exposed at the air sampler station
r = dose rate in mr/hr at H + 1 hour from monitor readings
C_F = counting rate for the air sample filter

Two air samplers were located on the large YCV barge at Station S-6, and results are listed for both.

For each air sampler, the average of the counting rates for all sticky pans located on each barge was used for C_S for one calculation, and the dose rate as measured by monitors was used for the other. For two stations (W-4 and W-8), the filter counting rates were below the mean background counting rate, and for another the "signal" was only about 8 percent of background. For these stations, no calculations were attempted.

The difference shown from two air samplers located at Station S-6 indicates that a much larger air volume should be filtered to gain a representative sample. Also, for such low contamination levels as experienced over the lagoon part of the array, it is doubtful if 8- by 1-inch sticky pans have a reasonable probability of collecting a representative sample. Probable error in dose rate, determined by a single sticky-pan reading, is certainly higher when monitor dose-rate readings and sticky-pan readings from the barges are compared.

By use of the average value of $\bar{f}$ for each of the two closest barge stations and on the assumption that the collected particles originated from the vertical axis of the visible cloud, a range of contributing altitudes in the cloud was defined as listed in Table 3.4. This altitude range was determined graphically from Figure 3.4 by constructing lines with slopes equal to the average values of $\bar{f}$ through points corresponding to time of arrival at the barge stations. The intersection of these lines with Curves h_1 and h_3 defined the range of contributing altitudes. A windspeed of 15 knots was used for this determination. A range of times for the start of free fall by collected particles is also indicated by this procedure.

It was hoped that it would be possible to use these measurements to help indicate the proper approach to the problem of constructing a dynamic model for close-in fallout computation. Specifically, it was desired to test the assumption that particles are released

from the rising cloud when their fall rate is equal to the rise rate of the cloud.

Results from the small barge are not inconsistent with this assumption, since, during the interval from H + 0.5 to H + 1 minute, cloud rise rates of 1,700 to 454 feet per minute were measured for the upper and lower parts of the cloud.

This is not the case for the YCV barge at Station S-6, however. For the interval between 0.1 and 0.6 minute, the lowest rise rate associated with the visible part of the cloud was 570 ft/min, which is over twice the value of $\bar{f}_{av}$. Still, the large difference between the amounts of activity collected by the two adjacent air samplers suggests that a large error could be associated with the fall-rate calculation, large enough even to accommodate the above assumption.

It must be concluded that these air sampler results are too uncertain for anything more than speculation.

3.10 FALLOUT COMPARISONS

In the first chapter, estimates were made of fallout to be expected from a surface burst by scaling results from other shots. Figure 3.14 compares these estimates with estimates based on measurements from Shot Fig. Values from Fig fall considerably below estimates from higher yields.

The scaling techniques of Reference 1, which depend on assumptions enumerated in Section 1.2.2, lead to gross overestimates of downwind extent for H + 1 hour dose rates of 100 r/hr and lower. Also, the percentage of total activity deposited within the Fig array is estimated by this source to be 12 percent as compared to the 4 percent estimate based on measurements. Results from the 1.2-kt surface detonation of Operation Jangle form the basis for estimates in Reference 1, together with the so-called cube-root scaling procedure. It is interesting to speculate on the reasons for failure of the scaling method to predict better the fallout from Shot Fig. Cloud dimensions for the two events, Jangle Surface and Fig, did not scale as the cube root of yield. The ratio of cloud heights, for example, was about 2 to 1, This would cause cube-root scaling to provide an overestimate of intensities.

Also, in the case of Shot Fig, the cloud drifted across the entire instrumentation array before stabilization occurred. Since the amount of time required for cloud stabilization is independent of yield, drift during cloud rise could cause failure of scaling methods that do not account for it, especially if, as in this case, scaling is to be made for distances that are not large compared to the drift of the cloud during stabilization.

To gain a better indication of the significant differences in fallout from Fig and Jangle Surface, a comparison was made of the percentage of activity deposited within comparable distances for the two shots, accounting for actual cloud heights and drift of the cloud during its rise.

The downwind distance d of a particle is the vector sum of the distance covered during rise and the distance covered during fall as follows:

$$\vec{d} = \vec{u}_R t + \vec{u}_F \frac{h}{f} \qquad (3.1)$$

Where: u_R = effective mean wind velocity during particle rise

$\vec{u}_F$ = effective mean wind velocity during particle fall

h = altitude where the particle with fall rate f starts free fall at time t

Since cloud rise is not constant, $\vec{u}_R$ is not necessarily equal to $\vec{u}_F$.

For the special case of a wind-height structure with no shear in direction or speed,

$$d = u\left(t + \frac{h}{f}\right) \tag{3.2}$$

Since Fig wind conditions were nearly this, it was assumed that Equation 3.2 was applicable for Fig data.

The value of d was determined for Fig by the length of the instrumentation array (10,500 feet). It was assumed that all fallout particles originated from the central point of the rising puff ($[h_2 + h_3]/2$, as shown in Figure 3.2). For various values of f, release heights and times were computed graphically (Figure 3.15). The height of the puff midpoint was plotted as a function of time. The point corresponding to time of arrival at 10,500 feet was located at 6.9 minutes on the abscissa, and lines with slopes corresponding to various chosen fall rates were constructed through that point. Intersections of fall-rate lines with the puff midpoint line gave the release height and time for each fall rate taken.

With the usual assumption of similar vertical distribution for activity, the corresponding release heights for Jangle Surface were determined by applying a factor of 2, which was the ratio of cloud heights for the two shots. With these values of h and t, a downwind distance d, for Jangle Surface corresponding to 10,500 feet, was obtained from Equation 3.1 for each fall rate originally chosen. For a given fall rate, the ratio of this distance to 10,500 feet is a distance scaling factor. Distance scaling factors were computed for a range of fall rates with the results shown in Figure 3.16. Jangle Surface winds used were taken from Reference 6 and are listed in Table 3.5. It was assumed that both clouds required the same time to reach a given relative height.

Distance scaling factors range from 1.7 for 40-knot fall rate to 0.8 for 2-knot fall rate. However, considering the rate of rise of the $(h_2 + h_3)/2$ point, it is unlikely that fall rates smaller than 5 knots made much of a contribution within the Fig instrumentation array. Thus, a scaling factor of 1.5 to 1.6 is probably a reasonable one to apply for comparison of the percentage of activity deposited. It can be seen from Equation 3.2 that, for comparison of two events having a cloud-height ratio of 2 to 1 under the same no-shear wind conditions, the distance scaling factor will approach 2 as fall rate increases and 1 as fall rate decreases. The relatively low wind speeds at low levels and high wind speeds at high levels for Jangle Surface have practically reversed this behavior.

Thus, if assumptions regarding similarity of activity distribution are valid, it would be expected that 4 percent of the fission product activity produced by Jangle Surface would be found within 17,000 to 16,000 feet of ground zero. However, when the Jangle Surface pattern is integrated out to this downwind distance, it is found that 6 percent of the activity is accounted for. This small variance is believed to be indicative of a real difference in relative activity distribution for the two shots, in spite of the fact that measurements were somewhat inadequate over the lagoon part of the instrumentation array during Shot Fig.

The primary reason for this conviction is that about 3 percent of Fig activity was accounted for within the 100-r/hr contour, largely over well-instrumented land. For fallout over the lagoon to account for 3 percent rather than 1 percent, a large consistent error in many individual measurements would be required.

However, such a difference is not surprising, considering the difference in yield for the two shots. Also, the difference is such as to make low-yield fallout less of a military problem.

The interesting side of this result is whether the same sort of behavior extends farther up the yield scale. Yields 10^6 times greater than Fig are to be considered.

Assumptions regarding similarity of vertical space distributions for activity and fall-rate distribution of activity might also be questioned on inductive grounds. These two

assumptions seem to be contradictory in view of certain facts concerning cloud rise. For example, the rise rate of clouds increases with yield. If the activity is associated with the same particle-size distribution for all yields, it would seem that particles of a given fall rate would be left behind the rising cloud at relatively lower cloud heights for smaller yields. Thus, if there is only one fall-rate distribution for all yields, vertical distribution of activity should differ for different yields.

However, it is known that the speed of turbulent after-winds, which draw in and mix debris with active material inside the fireball, increases with yield. Thus, for a larger yield, a particle of given cross section sweeps out a greater volume in a given time and has a correspondingly higher probability of colliding with other particles to form relatively large fallout particles. Thus, it seems likely that the usual assumptions regarding vertical activity distributions and activity fall-rate distribution are both wrong for close-in fallout.

The errors produced are apparently such that close-in fallout intensity is underestimated by scaling from small yields to large yields. Within the available experience for one type of surface, the larger the yield difference, the larger the scaling error.

An interesting question from a military point of view is whether this apparent trend is real and continues up the scale of yield into the megaton range. If so, the present estimates of close-in intensities from megaton yields could be significantly low.

3.11 DYNAMIC FALLOUT MODEL

Only about 4 percent of the total activity produced by Shot Fig was accounted for within the instrumentation array. However, this included all of the activity associated with fall rates great enough to cause intensity levels of military interest. For these reasons, only 4 percent of the total activity produced is incorporated in the dynamic fallout model proposed for use with any wind structure to estimate close-in fallout from fission weapons of 1- to 100-ton yield. The main features of the model are:

1. Fall-rate distribution for the activity (3×10^6 r/hr-ft^2 per ton of fission yield) is log normal with $\sigma = 0.48$ and $f_0 = 24$ knots. That is,

$$\phi(f) = \frac{1}{\sqrt{2\pi}\sigma f} e^{-\frac{1}{2\sigma^2}\left[\ln \frac{f}{f_0}\right]^2}$$

Where: $\phi(f)$ = fraction of activity associated with the fall-rate range f to f + df.

2. All activity is associated with that part of the visible cloud that corresponds to the region between h_2 and h_3 shown in Figure 3.2. Scaling of h_2 and h_3 with yield should be made by a $\frac{1}{4}$-power law using Fig data as the basis. Scaling for diameter should be made by a $\frac{3}{8}$-power law. For all yields, equal time is required for h_2, h_3, and diameter to reach a given fraction of their maximum values.

3. Activity is assumed to rise until the rise rate of the cloud corresponds to the fall rate of the activity, at which point free fall commences.

This model is reasonably consistent with the measured amount of activity deposited as a function of downwind distance, intensity as a function of downwind distance, cloud shine measurements, and cloud drift and growth for Shot Fig.

Calculations have been made that utilize these assumptions and some approximations to allow relatively easy hand computation. The Fig yield and cloud dimensions were

used, but a no-shear wind condition was taken. Results are shown in Figure 3.17 for windspeeds of 5, 15, and 30 knots. The downwind extent of the 10-r/hr level more than doubles with increase in windspeed from 5 to 30 knots; however, the 100-r/hr extent is fairly insensitive. Close-in intensities greater than 100 r/hr show an increase in extent with windspeed decrease.

TABLE 3.1 DOSE-RATE DECAY

Station	Number of Readings	Time Interval (hours after zero time)	Inferred Dose-Rate-Measurement Error, Assuming $t^{-1.1}$ Decay	Station	Number of Readings	Time Interval (hours after zero time)	Inferred Dose-Rate-Measurement Error, Assuming $t^{-1.2}$ Decay
			percent				percent
B-10	3	3.4 to 46	± 18	I-40	3	1.1 to 8.5	± 62
B-20	5	1.7 to 47	± 30	I-50	3	0.8 to 8.5	± 34
B-45	4	1.0 to 3.3	± 20	I-60	3	1 to 8.5	± 15
B-60	3	0.6 to 3.3	± 49	I-70	3	1 to 8.5	± 29
C-30	3	0.8 to 8.5	± 42	J-20	4	3.5 to 47	± 35
C-45	4	0.8 to 8.5	± 15	J-30	3	1.7 to 8.5	± 36
D-20	6	1.7 to 46	± 61	J-40	3	1.7 to 8.7	± 14
D-30	3	0.8 to 8.5	± 10	J-50	4	1.7 to 8.5	± 20
E-10	3	3.5 to 48	± 4	J-60	3	1.8 to 8.5	± 8
E-20	4	3.5 to 47	± 2	J-70	6	0.8 to 8.5	± 25
G-25	3	3.5 to 46	± 19	K-20	5	1.6 to 46	± 34
G-30	3	3.5 to 46	± 30	K-30	3	1.6 to 8.5	± 38
G-35	3	3 to 9	± 14	K-45	3	1.6 to 8.5	± 30
H-20	3	3.5 to 47	± 30	K-60	3	1.5 to 8.5	± 65
H-40	3	1.1 to 3.4	± 22	K-75	4	1.4 to 8.5	± 25
I-20	5	2.2 to 46	± 19	Crater lip	7	3.3 to 48	± 198
I-30	4	1.2 to 8.5	± 15				

TABLE 3.2 STICKY-PAN MEASUREMENTS

Station	Sticky Pan Gamma Counting Rate at H + 3 Hours	Inferred Dose Rate From Sticky Pan at H + 1 Hour	Measured Dose Rate at H + 1 Hour
	counts/min	r/hr	r/hr
B-60	15,800	1.3	0.83
BB-55	3,080	0.24	1.2
C-45	51,600	4.1	2.3
H-40	293,000	23	35
I-30	368,000	29	32
I-40	172,000	14	10
I-50	49,300	3.9	5.3
I-60	18,300	1.5	2.8
I-70	14,900	1.2	1.9
J-60	31,800	2.5	2.1
J-70	15,000	1.2	1.2
J-100	4,650	0.37	0.4
J-150	2,000	0.16	0.056
K-45	54,500	4.4	6.3
K-60	20,000	1.6	2.0
K-75	11,000	0.88	0.36
K-100	3,410	0.27	0.27
K-150	700	0.056	0.028

TABLE 3.3 PLUTONIUM MEASUREMENTS

Station	Inferred Gamma Dose Rate*	Measured Plutonium Contamination†	Ratio
	r/hr at 1 hr	μgm/m²	$\frac{r/hr}{\mu gm/m^2}$
I-30	29	4.7	6.2
I-40	14	17	0.78
I-60	1.5	30	0.048
I-70	1.2	0.10	12
J-60	2.5	0.023	109
J-100	0.37	0.020	18
K-100	0.27	0.097	2.8
A-2	—	0.032	—
H-40	23	3.6	6.4
BB-55	0.24	0.064	3.7
N-6	0.068	40	1.7×10^{-3}
N-6	0.068	1.6	0.042
O-6	0.05	0.57	0.088
R-5	—	0.10	—
S-6	0.012	0.067	0.18
Y-4	0.16	0.22	0.73
Z-4	0.09	0.17	0.53

* From gamma-counting sticky pans.
† Radiochemistry.

TABLE 3.4 FALL-RATE MEASUREMENTS

Station	Approximate Range	Mean Time of Arrival	Filter Counting Rate	Background Counting Rate	C_F Filter Counting Rate Minus Background	$\bar{f}$ Computed From Sticky-Pan Results	$\bar{f}$ Computed From Monitor Dose Rate Measurements	$\bar{f}_{av}$	Apparent Range of Contributing Heights	Range of Times for Start of Fall
	ft	min	counts/min at H + 3 hours	counts/min at H + 3 hours	counts/min at H + 3 hours	ft/min	ft/min	ft/min	ft	min
Small barge P-5	2,300	1.5	641	117 ± 8	524					
YCV barge S-6	3,800	2.4	381	117 ± 8	264					
			188	117 ± 8	71					
YC barge W-4	7,800	5.0	105	117 ± 8	0					
YC barge W-6	7,700	5.0	126	117 ± 8	9	—	—			
YC barge W-8	7,700	5.0	92	117 ± 8	0	—	—			

TABLE 3.5 JANGLE SURFACE WINDS

Altitude Above MSL	Direction	Speed
feet	degrees	knots
Surface	190	2
4,213	170	13
6,000	180	26
8,000	200	32
10,000	200	37
12,000	210	40
14,000	210	44
16,000	200	63
18,000		

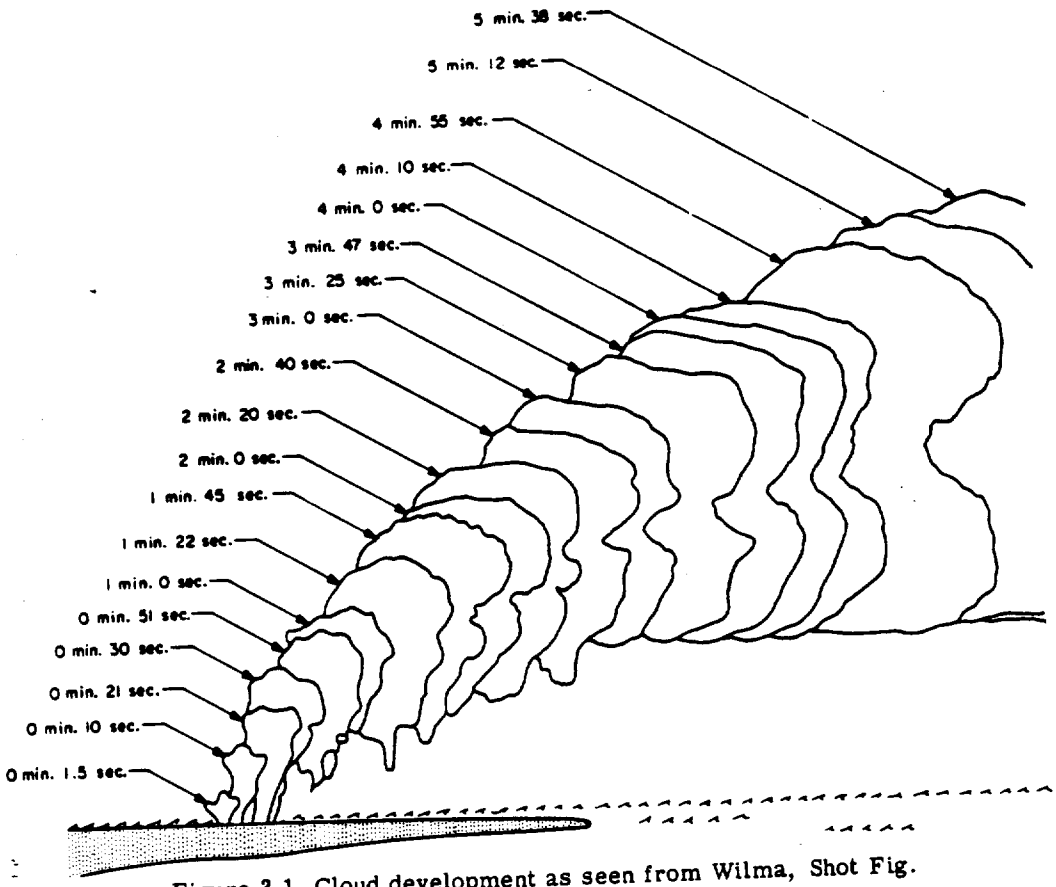

Figure 3.1 Cloud development as seen from Wilma, Shot Fig.

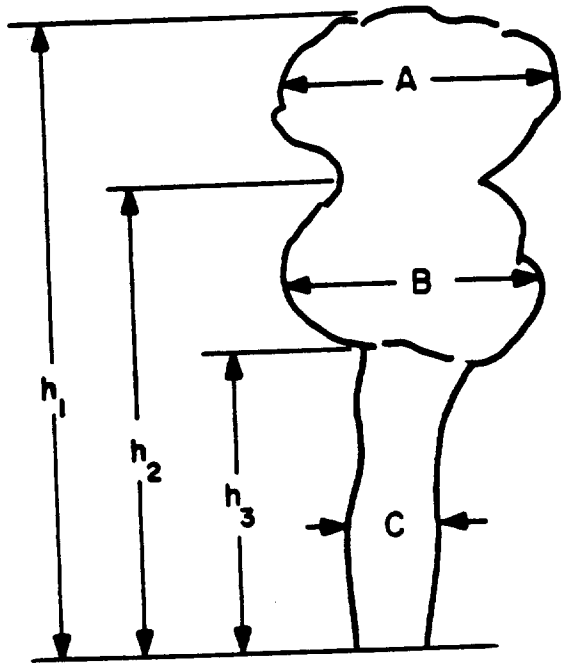

Figure 3.2 General features of the cloud.

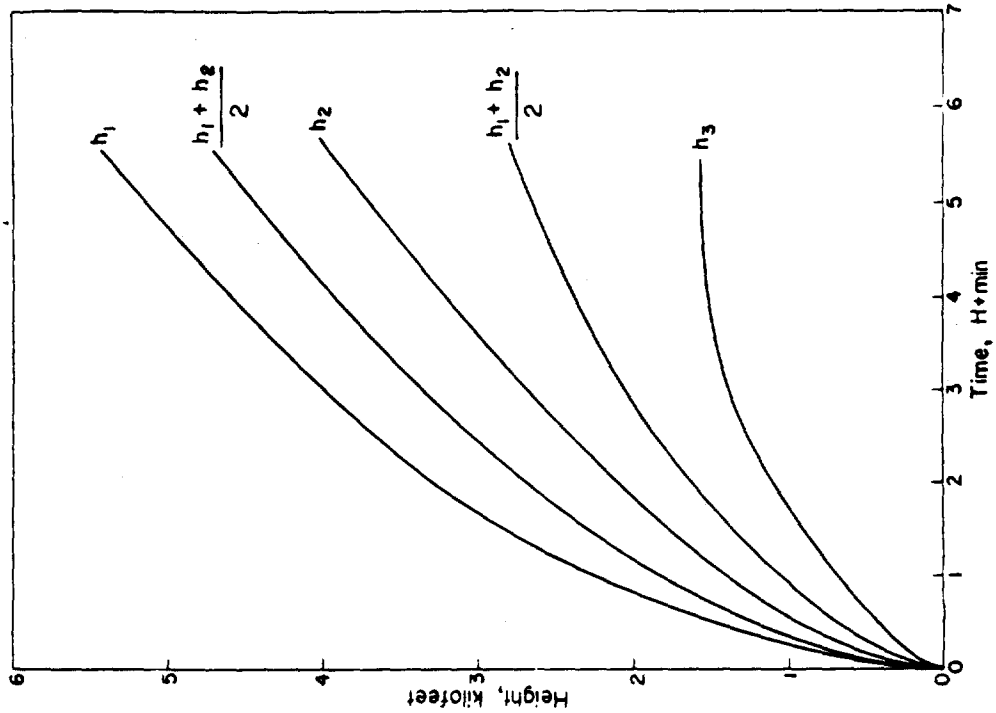

Figure 3.4 Cloud height versus time.

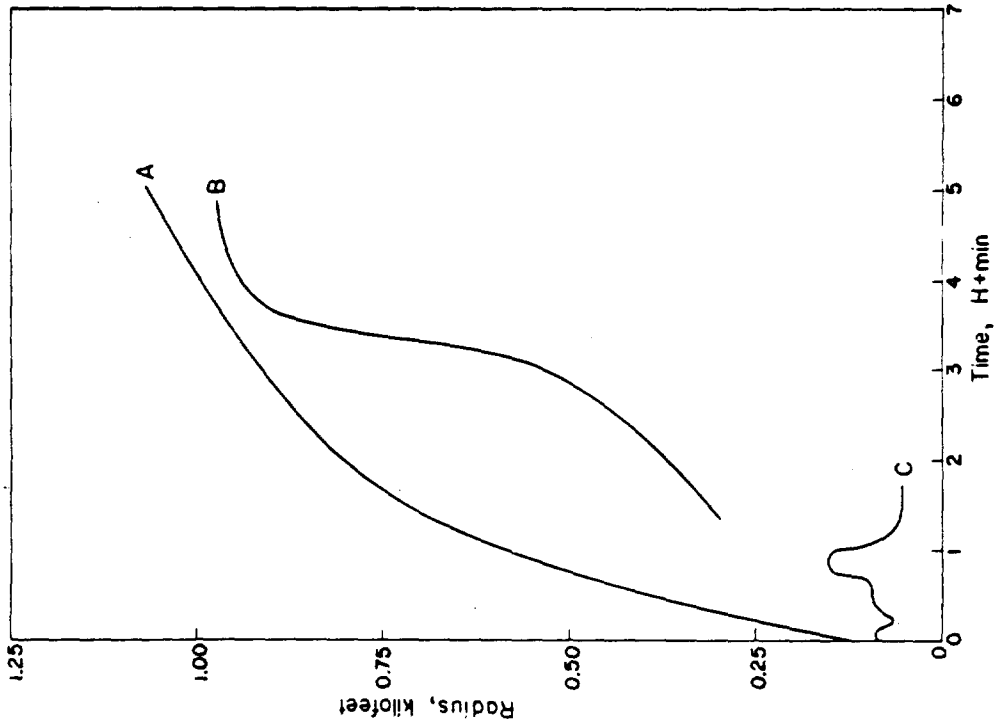

Figure 3.3 Cloud radius versus time.

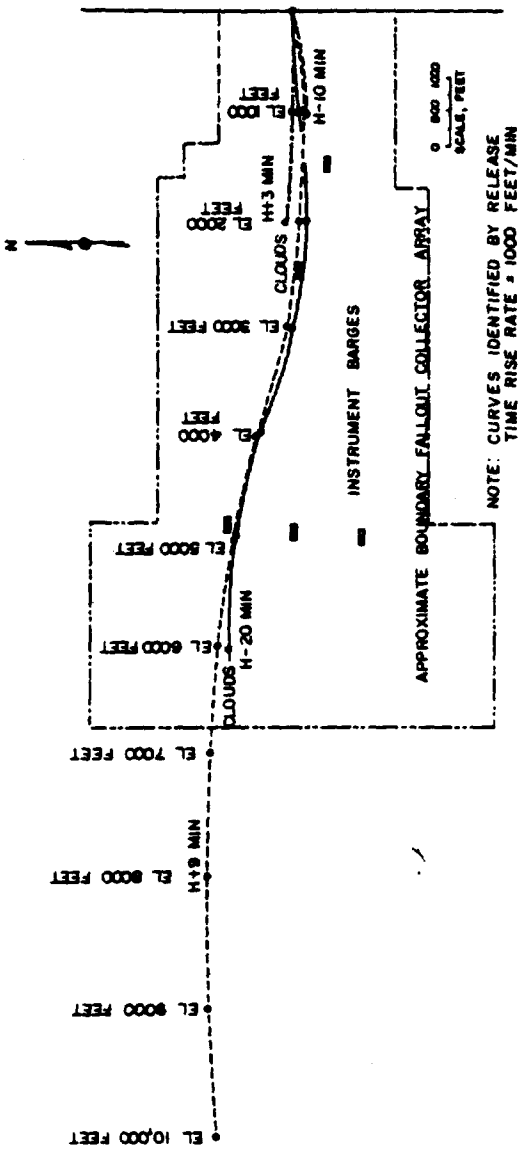

Figure 3.5 Wind conditions, Shot Fig.

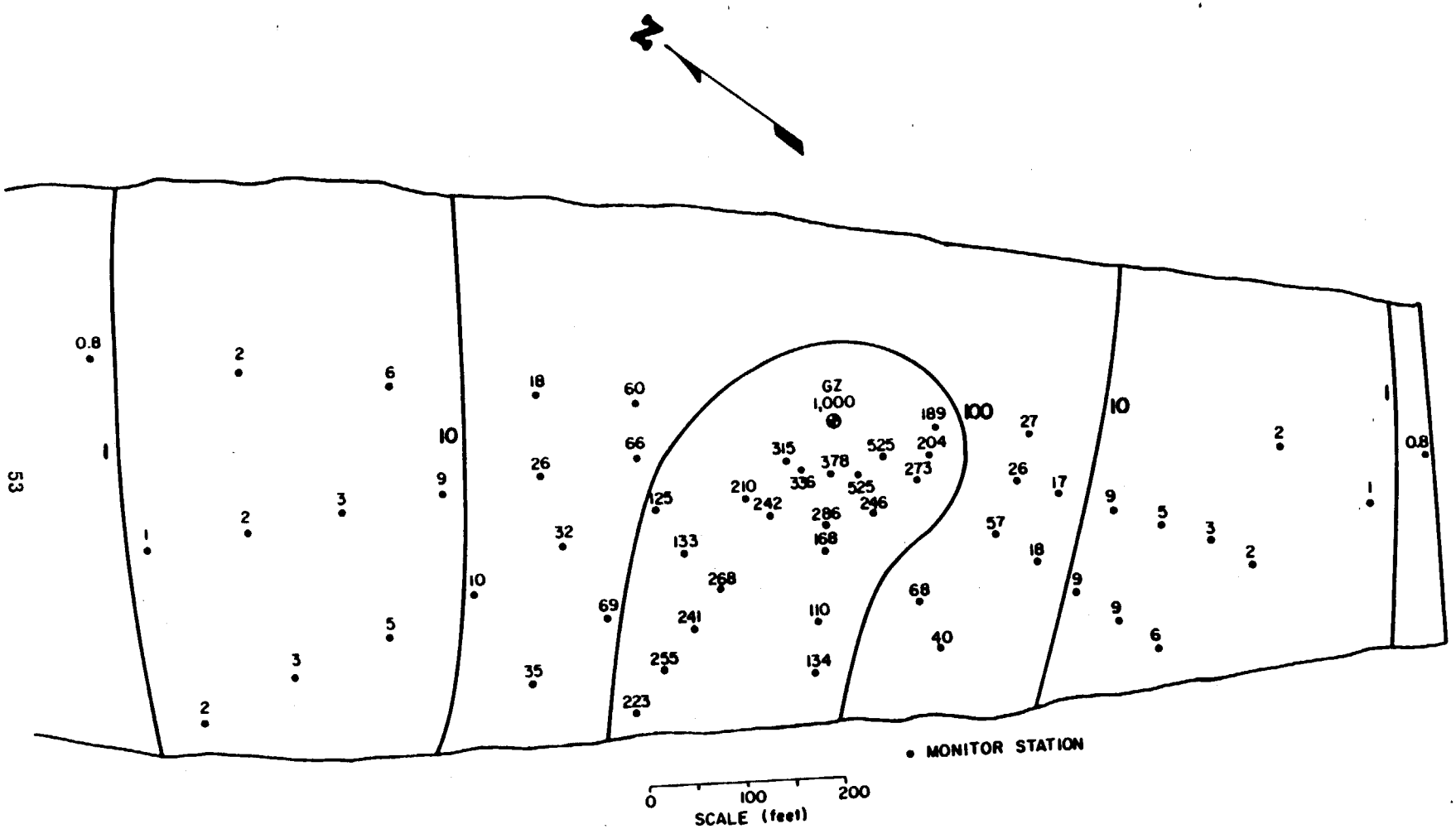

Figure 3.6 Dose rates (r/hr) on land at H + 1 hour.

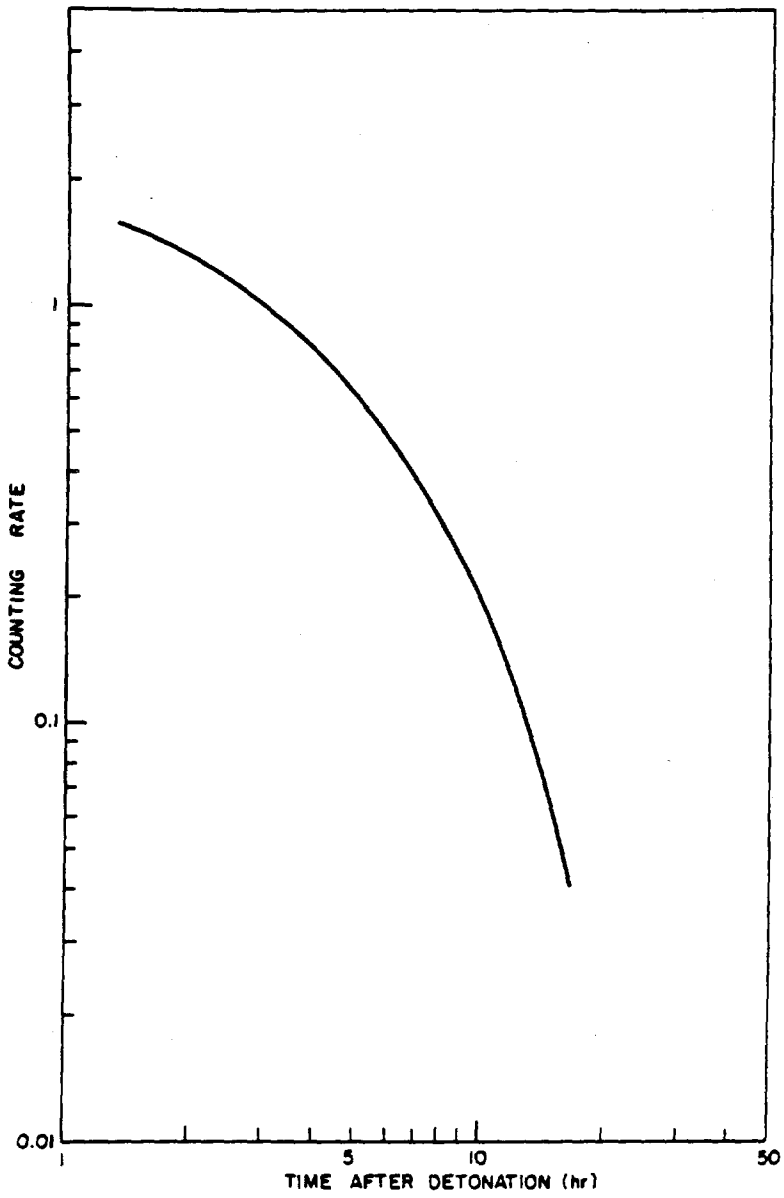

Figure 3.7 Sticky-pan decay curve.

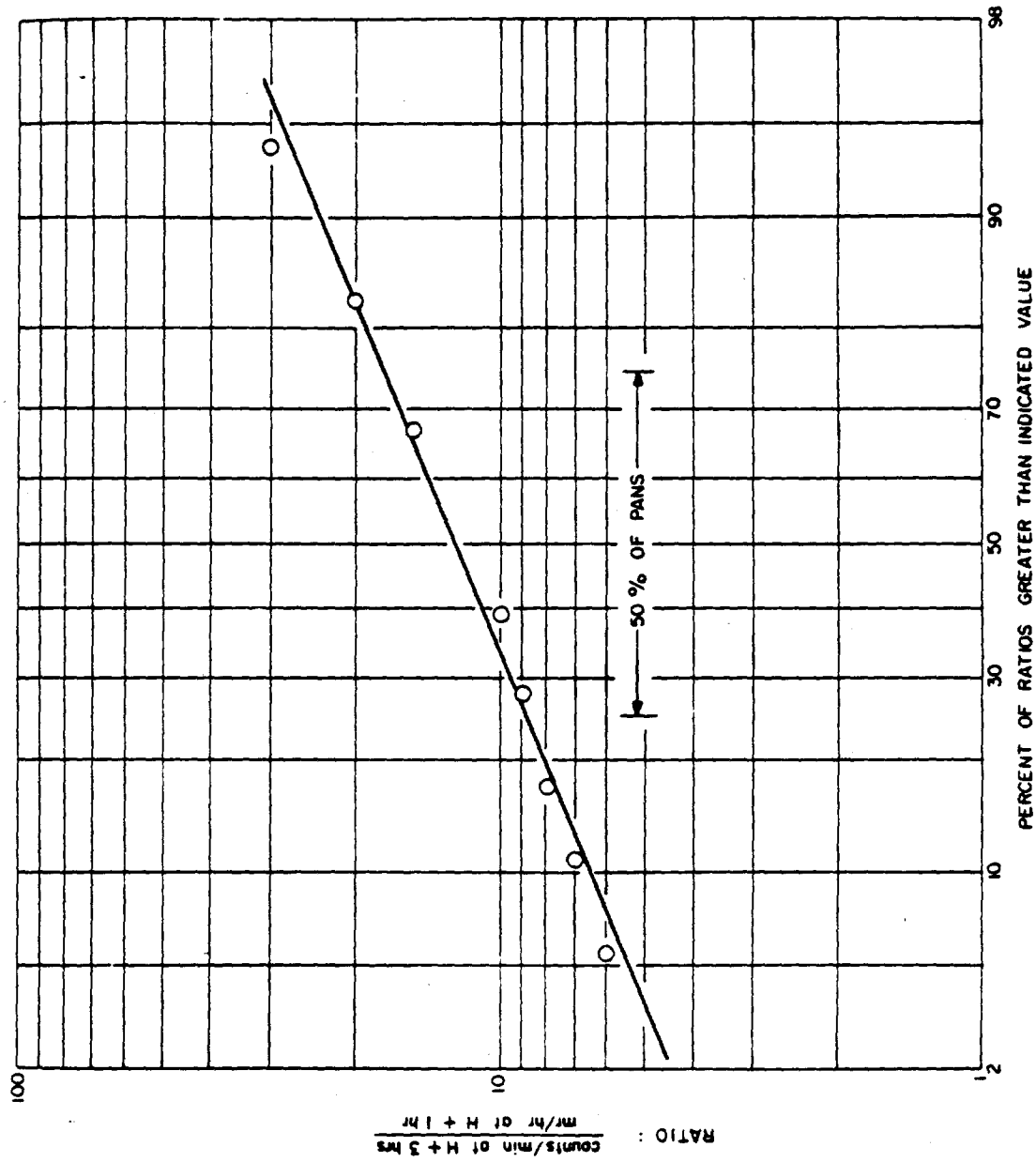

Figure 3.8 Comparison of monitor and sticky-pan results.

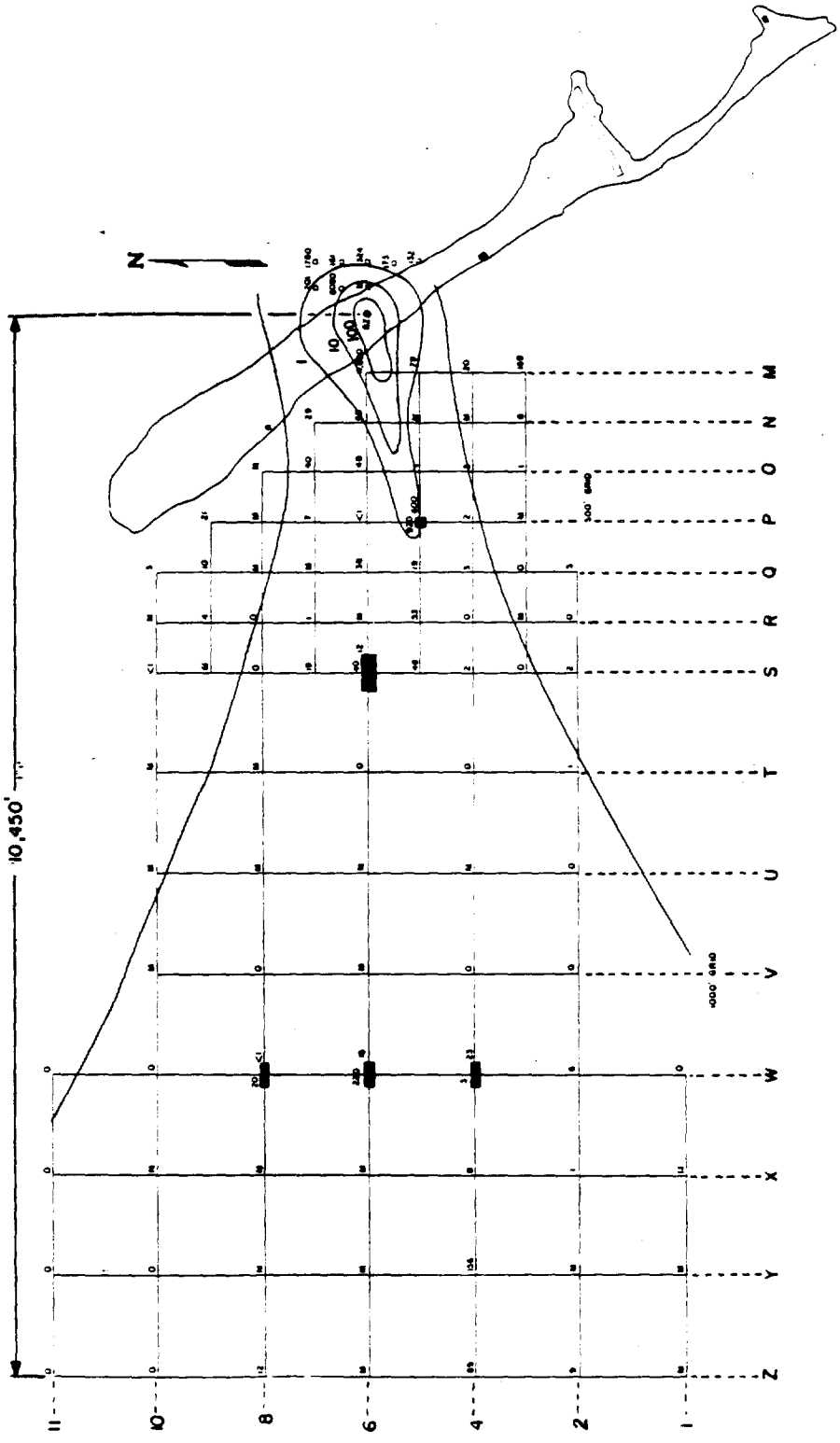

Figure 3.9 H + 1 hour dose-rate contours for complete array.

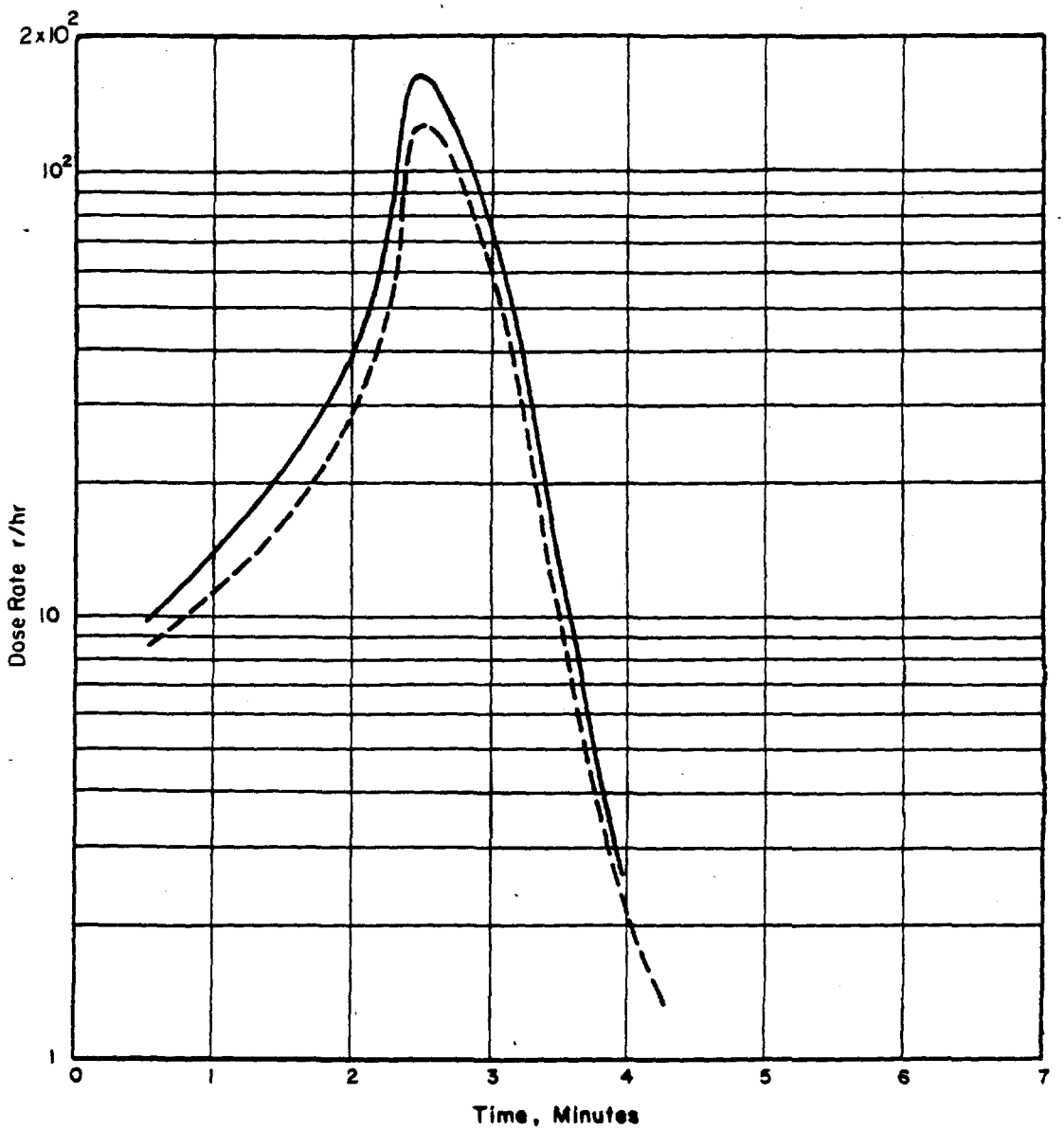

Figure 3.10 Cloud shine on YCV barge.

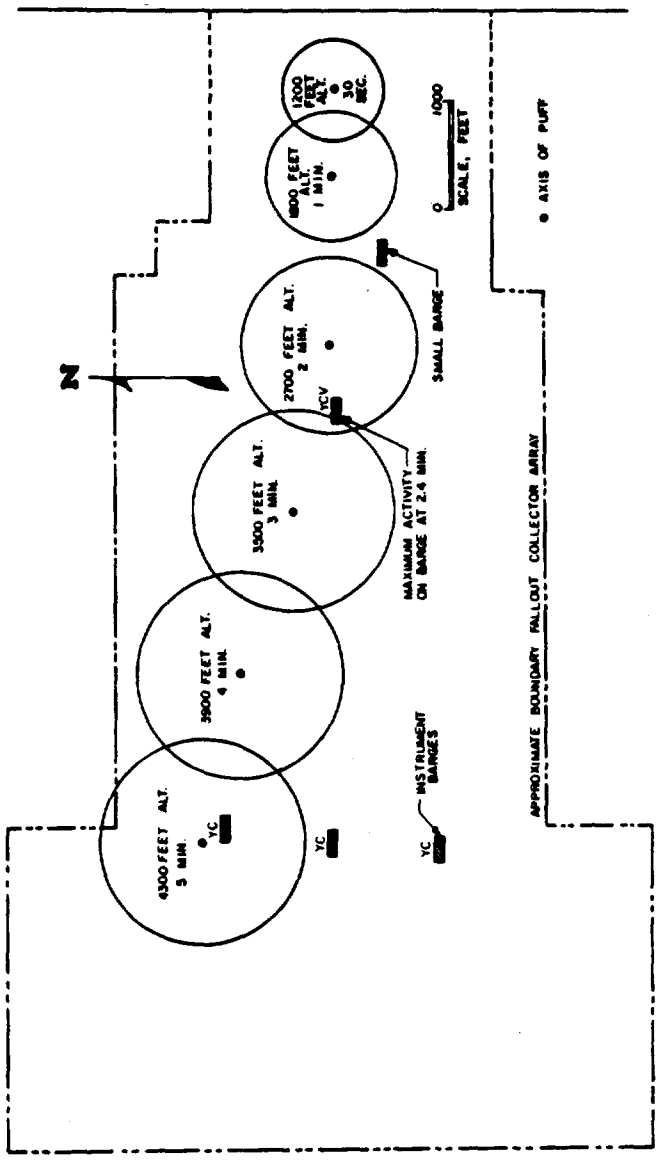

Figure 3.11 Puff trajectory.

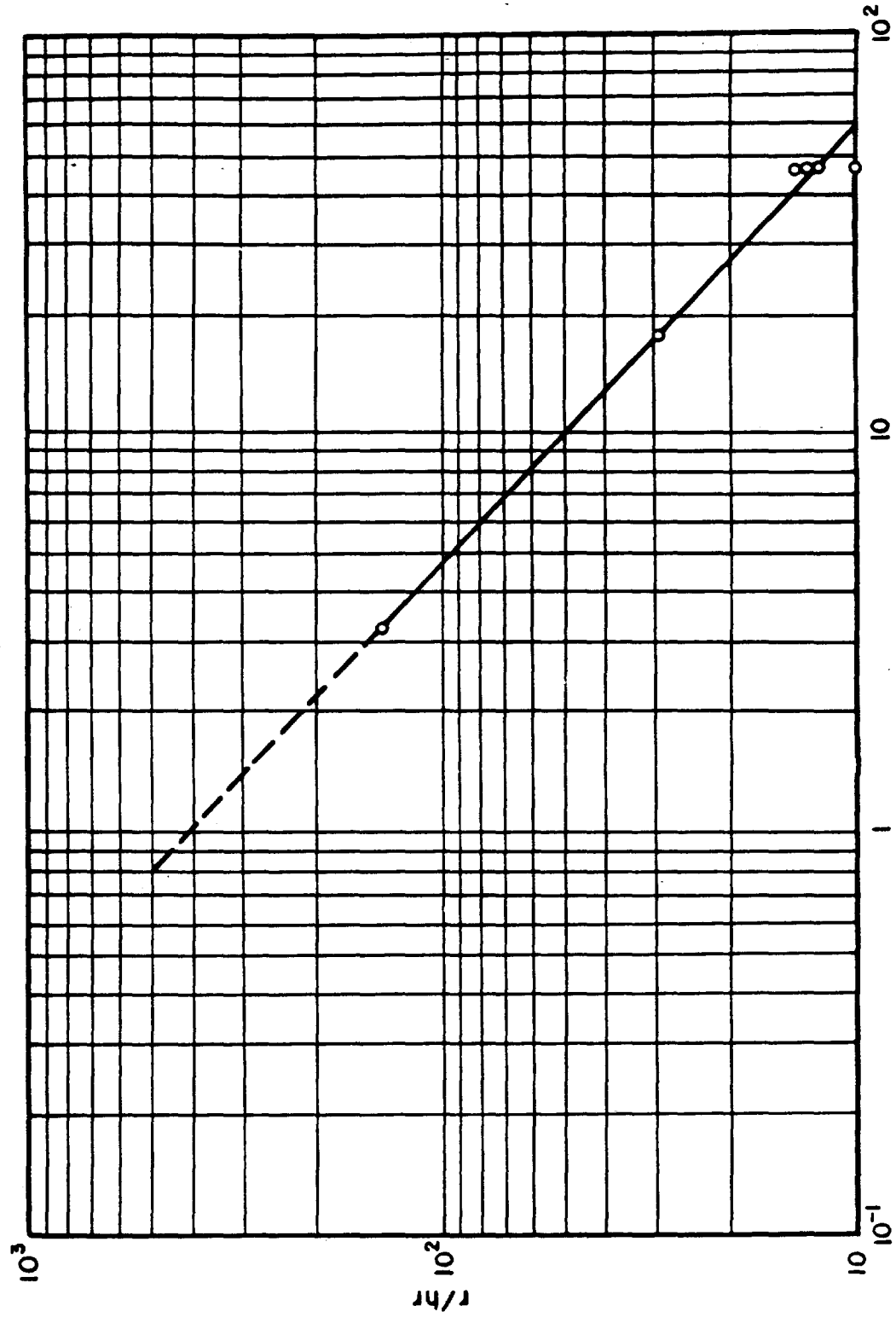

Figure 3.12 Crater data.

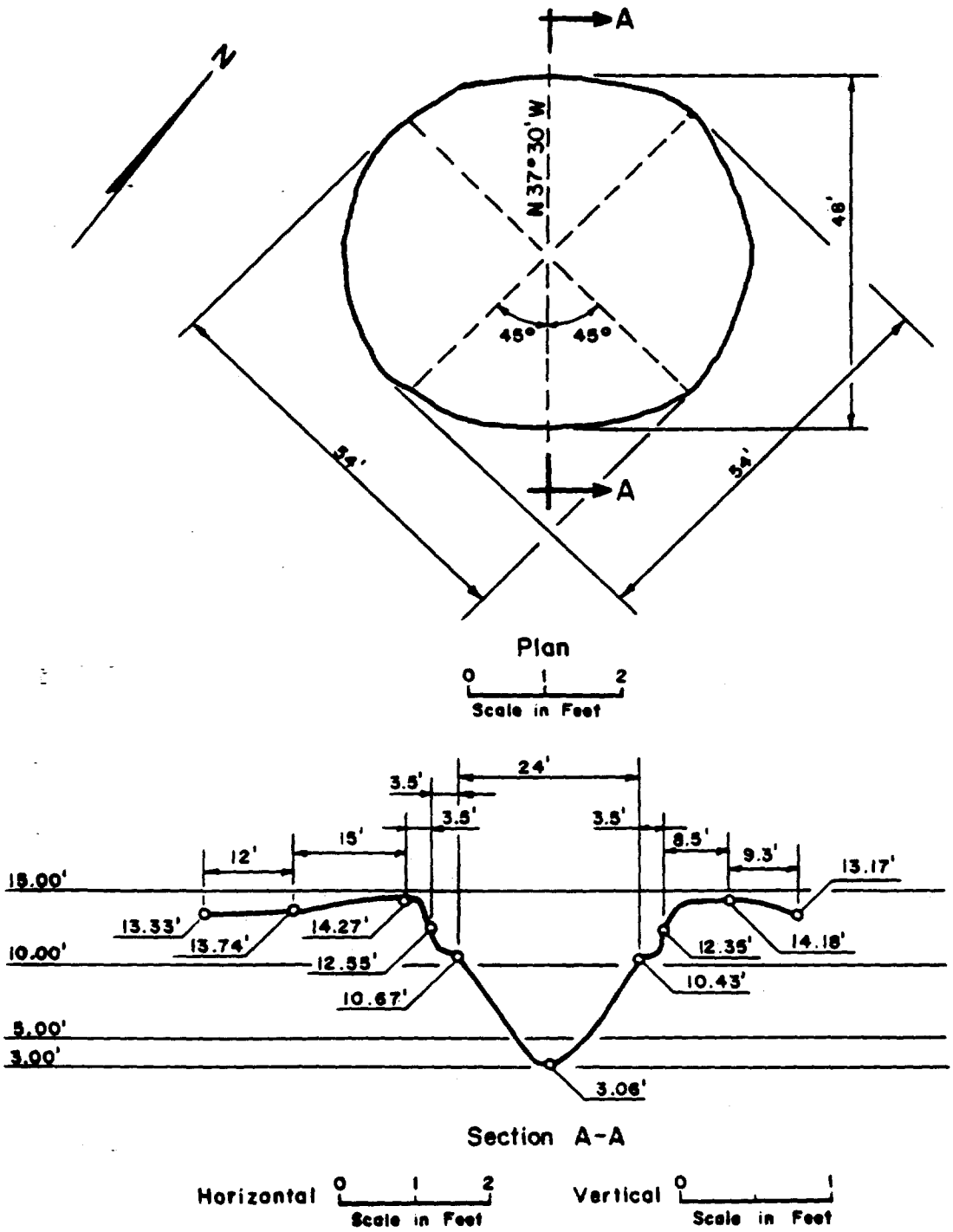

Figure 3.13 Survey of Fig crater on D + 3 days; original ground level, 12.85 feet.

Page 61 deleted.

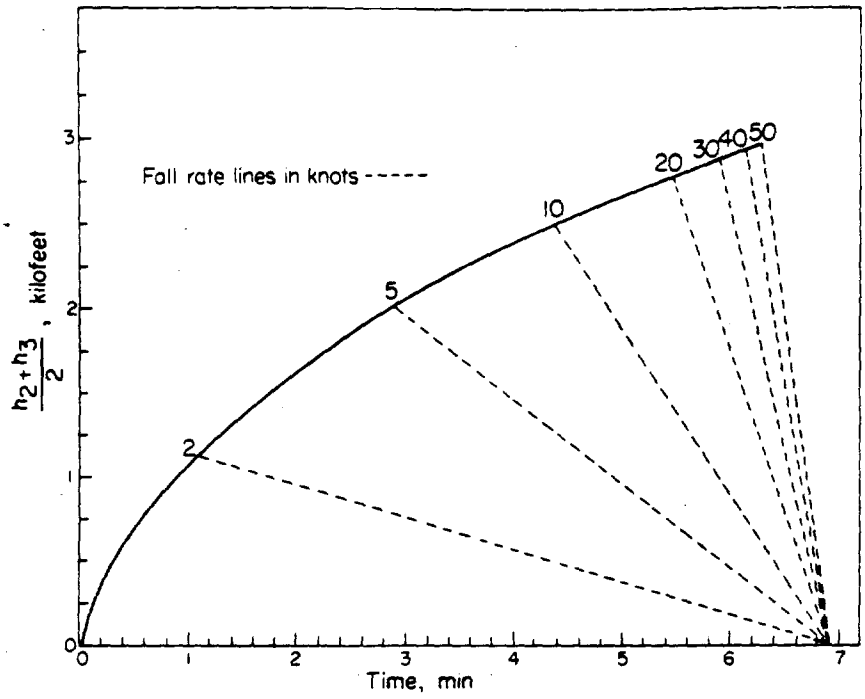

Figure 3.15 Release heights for various fall rates, Shot Fig.

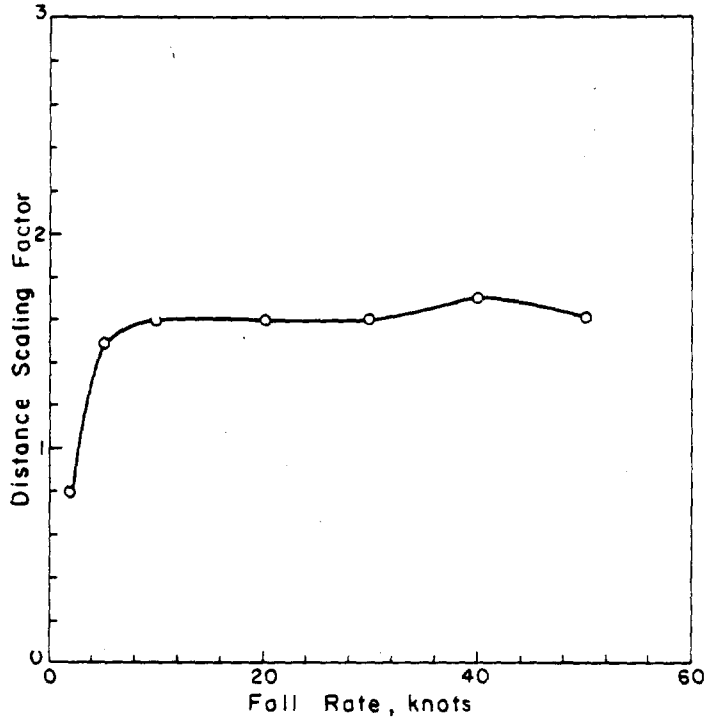

Figure 3.16 Distance scaling factors for Jangle Surface and Shot Fig.

Page 63 deleted.

Chapter 4

CONCLUSIONS AND RECOMMENDATIONS

Shot Fig provided sufficient data to determine the general characteristics of fallout of military importance for small yields.

The scaling techniques in Reference 1 lead to gross overestimates of downwind extent for H + 1 hour dose rates of 100 r/hr and lower for the particular conditions of Shot Fig (15-knot winds). Apparent reasons for the failure are: (1) Cloud height for Shot Fig was considerably greater than that implicitly assumed by the scaling technique. (2) No accounting is made for the drift of the cloud during its rise. (3) Activity distributions with height and fall rate are not similar over the large yield range involved. Scaled estimates are more nearly correct for intensities greater than 100 r/hr.

A dynamic fallout model is proposed (Section 3.11) to estimate close-in fallout from fission weapons of 1- to 100-ton yield. This model accounts for cloud drift and growth and is consistent with Fig measurements of the amount of activity deposited as a function of downwind distance, intensity as a function of downwind distance, and cloud shine.

Calculations made on the basis of this model show that intensities greater than 100 r/hr increase in downwind extent as windspeed decreases, whereas intensities less than 100 r/hr reverse this behavior. This is not consistent with present techniques of accounting for variation in windspeeds where the downwind extent of any intensity is increased with the increase of windspeed. It is recommended that the dynamic model be used to estimate effects of windspeed variation.

Winds that existed during Shot Fig exhibited a very small directional shear, and mean windspeeds ranged from 11 to 16 knots when averaged from pertinent altitudes to the surface. The visible cloud had not reached its ultimate height of 6,000 feet by the time it had drifted beyond the instrumentation array, some 10,500 feet from ground zero.

Only 4 percent of the fission products formed was accounted for within the array. From cloud shine measurements, it was deduced that most of the activity was carried beyond the array in the lower portion of the visible cloud between 0.3 and 0.7 of its maximum height.

The earliest measurement obtained within the crater itself was at H + 3.5 hours, at which time a monitor descended inside the crater lip and recorded about 140 r/hr on the Jordan survey meter. This reading implies an intensity less than 1,700 r/hr at H + 26 minutes, which is a much lower value than that reported in Reference 7. Cave-in of the crater walls could have been responsible for this apparent inconsistency.

The use of $t^{-1.2}$ decay law will generally lead to errors no greater than those involved with dose-rate measurement in the field and is recommended for field use.

Although only a few plutonium contamination measurements were made during Fig, the levels were low enough to indicate that no serious long-term problem would result from this source.

As expected, it was difficult to make completely definitive fall-out radiation measurements without the ability to make full-field dose-rate measurements at any point within the instrumentation array. Use of sticky-pan fallout collectors gave results reasonably consistent with survey meter readings for the high-intensity regions that resulted on the shot

island. A probable error of ±50 percent was indicated in this region. For the low-inten regions of the lagoon, a much larger error was indicated. The use of large barges to co lect fallout for gamma survey measurements aids in fallout studies that have to be con- ducted over water. If the experiment were repeated over water areas, more extensive u should be made of flat-topped barges.

REFERENCES

1. "Capabilities of Atomic Weapons"; Department of the Army Technical Manual TM 23-200, Department of the Navy OPNAV Instruction 03400.1B, Department of the Air Force AFL 136-1, Marine Corps Publications NAVMC 1104 Rev; Revised Edition, November 1957; Prepared by Armed Forces Special Weapons Project, Washington, D.C.; Confidential.

2. C. F. Ksanda and others; "Scaling of Contamination Patterns, Surface and Underground Detonation"; USNRDL-TR-1, 15 Sep 1953; Naval Radiological Defense Laboratory, San Francisco, California.

3. M. Cowan, Jr.; "Plutonium Contamination from One-Point Detonation of an XW-25"; Program 71, Test Group 57, Operation Plumbbob, WT-1510, November 1960; Sandia Corporation, Albuquerque, New Mexico; Secret Restricted Data.

4. W. E. Knabe and G. E. Putnam; "The Activity of the Fission Products of U^{235}"; January 1959; General Electric Atomic Products Division, Cincinnati, Ohio.

5. P. J. Dolan; "Theoretical Dose Rate Decay Curves for Contamination Resulting from Land Surface Burst Nuclear Weapons"; DASA-528, 6 Aug 1959; Headquarters, Defense Atomic Support Agency, Washington, D.C.

6. E. H. Karstens; "Air Weather Service Participation in Operation Jangle"; Project 1(8)b, Operation Jangle, WT-361, December 1951; Air Weather Service, Armed Forces Special Weapons Project, Washington, D.C.; Unclassified.

7. M. Morgenthau and M. Schumchyk; "Residual Radiation from a Very-Low-Yield Burst"; Project 2.10, Operation Hardtack, WT-1678, December 1960; U.S. Army Chemical Warfare Laboratories, Army Chemical Center, Maryland; Secret Restricted Data.

Pages 67 and 68 deleted.